

¹ Investigation of the causes of historical changes in the ² sub-surface salinity minimum of the South Atlantic

Marlos Goes,¹ Ilana Wainer,² and Natalia Signorelli²

Corresponding author: Marlos Goes, CIMAS/University of Miami and NOAA/AOML, Miami, USA. (marlos.goes@noaa.gov)

¹CIMAS/University of Miami and NOAA/AOML, Miami, USA.

²Institute of Oceanography, University of São Paulo, São Paulo, Brazil

3 **Abstract.**

4 In this study we investigate the sub-surface salinity changes on decadal
5 timescales across the Subtropical South Atlantic Ocean using two ocean re-
6 analysis products, the latest version of the Simple Ocean Data Assimilation
7 and the Estimating the Circulation and Climate of the Ocean, Phase II , as
8 well as with additional climate model experiments. Results show that there
9 is a recent significant salinity increase at the core of the salinity minimum
10 at intermediate levels. The main underlying mechanism for this sub-surface
11 salinity increase is the lateral advective (gyre) changes due to the Southern
12 Annular mode variability, which conditions an increased contribution from
13 the Indian Ocean high salinity waters into the Atlantic. The global warm-
14 ing signal has a secondary but complementary contribution. Latitudinal dif-
15 ferences at intermediate depth in response to large-scale forcing are in part
16 caused by local variation of westward propagation features, and by compen-
17 sating contributions of salinity and temperature to density changes.

1. Introduction

18 Modulation and stability of the South Atlantic meridional overturning circulation are
19 dependent on salinity changes [*Weijer et al.*, 2002; *Peeters et al.*, 2004], and an improved
20 understanding of the mechanisms behind these salinity variations, especially the signature
21 of change below the ocean surface, is essential for better monitoring and prediction of
22 long-term climate change.

23 Long-term changes in ocean salinity are a function of large scale atmospheric forcing as
24 well as regional freshwater fluxes. In the South Atlantic Ocean, significant ocean warming,
25 which drives trends in freshwater fluxes, has been documented from observations and is
26 the subject of much research [*Gille*, 2002; *Curry et al.*, 2003; *Boyer et al.*, 2005; *Grodsky*
27 *et al.*, 2006; *Boning et al.*, 2008; *Schmidtko and Johnson*, 2012; *McCarthy et al.*, 2012].
28 Ocean salinity changes are in general depth and latitudinally dependent [*Curry et al.*,
29 2003]. They are larger in the top 500 m of the ocean because of the direct effect of
30 atmospheric fluxes. In comparison to earlier data on record (1960–1970s), more recent
31 years (1990s) have shown salinity increases in the tropical-subtropical latitudes due to
32 warming and increased evaporation [*Boyer et al.*, 2005], and salinity decreases in the
33 extratropical regions due to enhanced precipitation and runoff (including ice melting).

34 However, these long-term changes are subject to intense interannual and decadal vari-
35 ability [*Grodsky et al.*, 2006], and more recent data show an actual decrease in surface
36 salinity in the tropical Atlantic due to increased precipitation and upwelling. This impacts
37 the mixed layer depth, and therefore the formation of subsurface water masses.

38 Water masses that are formed on the base of the mixed layer are in contact with the
39 atmosphere for a relative short period during their formation. They are eventually sub-
40 ducted into the ocean interior following mostly an adiabatic pathway along neutral density
41 surfaces. At depth they are also modified by mixing which acts on much longer timescales.
42 Below the surface, the signature of salinity changes in the ocean is subject to higher un-
43 certainty than at the surface, since salinity is dynamically entangled with the temperature
44 field, which together determine the density [*Pierce et al.*, 2012]. Therefore, understanding
45 salinity changes in the South Atlantic at intermediate depths requires understanding the
46 relative contribution of the associated processes [*Durack and Wijffels*, 2010], such as sur-
47 face atmospheric forcing, circulation changes, changes due to mixing along the water-mass
48 pathways, and vertical movements of isopycnals due to wind field effects.

49 In the South Atlantic, an important impact of atmospheric forcing can be related to
50 changes in the Southern Annular Mode (SAM) through variations in sea level pressure
51 (SLP), which in turn would impact on the surface wind leading to a broad-scale sur-
52 face warming associated with the poleward migration of isopycnal outcrops [*Durack and*
53 *Wijffels*, 2010; *Schmidtko and Johnson*, 2012].

54 Although frequent in situ salinity data are scarce in the South Atlantic before 2002,
55 several studies have used historical ship-based conductivity– temperature–depth (CTD)
56 along with more recent Argo floats data to investigate long-term changes in the Sub-
57 Antarctic Mode Water (SAMW) and in the Antarctic Intermediate Water (AAIW) salin-
58 ity minimum layer underneath. Analysis of these data indicate cooling and freshening
59 of the SAMW, and warming and salinification associated with the AAIW [*Bindoff and*
60 *McDougall*, 1994; *Boning et al.*, 2008; *McCarthy et al.*, 2011; *Schmidtko and Johnson*,

61 2012]. Results also show a statistically significant shoaling of the isopycnals within the
62 circumpolar AAIW, accompanying a decrease in density, and an equatorward spreading
63 of the salinity anomalies at the sub-surface [*Durack and Wijffels, 2010; Schmidtko and*
64 *Johnson, 2012*]. A further decrease in the AAIW density is also projected for the 21st
65 century in climate models [*Goes et al., 2008*].

66 Further analysis of Argo observations reveals the variability of the AAIW salinity in the
67 South Atlantic on interannual and intradecadal timescales. Westward propagating salinity
68 anomalies at 30°S show that Rossby wave mechanisms are important for the interpretation
69 of salinity changes associated with the hydrological cycle of the AAIW at these timescales
70 [*McCarthy et al., 2012*].

71 In this study we investigate changes in the sub-surface salinity minimum of the South
72 Atlantic and its relation to large-scale trends such as those related to global warming
73 via greenhouse gases and the Southern Annular Mode (SAM). For this we use a blend of
74 ocean reanalyses and process oriented climate model experiments.

75 This paper is outlined as follows: Section 2 describes the two ocean reanalyses used
76 in this study; Section 3 shows the results of the examination of the two reanalysis data,
77 followed by the analysis of the climate model experiments. The setup of the climate
78 model experiments is presented in an Appendix; Sections 4 and 5 contain a discussion of
79 the results and the conclusion of this study.

2. Data

80 The first part of this study utilizes temperature and salinity data from the Simple Ocean
81 Data Assimilation (SODA) version 2.2.6 [*Ray and Giese, 2012*], and from the Estimating

82 the Circulation and Climate of the Ocean, Phase II (ECCO2). They can be described as
83 follows:

2.1. SODA 2.2.6

84 SODA 2.2.6 uses the Parallel Ocean Program (POP) model [Smith et al., 1992] at
85 a $1/4^\circ$ horizontal resolution, which is publicly available at an interpolated $0.5^\circ \times 0.5^\circ$
86 horizontal resolution, and 40 vertical levels at monthly averages, spanning the period of
87 1871 to 2008. Vertical diffusion of momentum, heat, and salt are carried out using K-
88 profile parameterization (KPP) mixing with modifications to address issues such as diurnal
89 heating, while lateral subgrid-scale processes are modeled using biharmonic mixing.

90 Surface boundary conditions used are from eight ensemble members of the NOAA atmo-
91 spheric Twentieth Century reanalysis 20Crv2 [Compo et al., 2011]. SODA 2.26 assimilates
92 only sea surface temperature (SST) data using a sequential estimation data assimilation
93 method [Carton and Giese, 2008]. The SST data comes from the ICOADS 2.5 SST prod-
94 uct (<http://icoads.noaa.gov>), which is based solely on in-situ observations (e.g., XBT,
95 CTD, bottle, Argo) and reached 2 million data report per year in the 1960s. Heat and
96 salt fluxes in SODA are calculated from bulk formulae using 20CRv2 daily variables.
97 By not assimilating in-depth hydrography and only SST, the model is more dynamically
98 consistent over different decades than alternative versions. A complete overview of the
99 ocean-reanalysis process is detailed by Carton and Giese [2008].

2.2. ECCO2

100 The Estimating the Circulation and Climate of the Ocean, Phase II (ECCO2) project
101 [Menemenlis, 2008]. An ECCO2 data synthesis is obtained by least-squares fit of a global

102 full-depth-ocean and sea-ice configuration of the Massachusetts Institute of Technology
103 OGCM [Marshall *et al.*, 1997] to the available satellite and in situ data. This least-
104 squares fit is carried out for a small number of control parameters using a Green’s function
105 approach [Menemenlis, 2005]. The solution requires the computation of a number of
106 sensitivity experiments that are free, unconstrained calculations by a forward model. The
107 experiments are designed to adjust the model parameters, forcing, and initial conditions.
108 Then the model is run forward again using the adjusted parameters, free of any constraints,
109 as in any ordinary model simulation. The model employs a cube-sphere grid projection
110 with a mean horizontal grid spacing of 18 km and 50 vertical levels. Surface forcings such
111 as wind and precipitation are from the JRA25 reanalysis [Onogi, 2007]. In the present
112 work, we use monthly average fields from January 1992 to December 2012.

3. Results

3.1. AAIW properties in SODA and ECCO2

113 As stated in the previous section, SODA 2.2.6 assimilates only SST data. This allows
114 the model to be more dynamically consistent over time, although larger differences may
115 exist with respect to actual hydrographic data. Salinity data in the South Atlantic are
116 historically sparse, mostly available in a more consistent way since the 2000s from Argo
117 floats measurements. ECCO2 uses a Green functions method, which also allows a smooth
118 salinity path over time, and allows a stronger hydrographic constraint with depth. We
119 estimate the differences in the representation of the AAIW in both reanalyses by com-
120 paring their salinity properties with an Argo climatology [Roemmich and Gilson, 2009],
121 which is available at a 1 degree horizontal resolution starting in 2004, for a similar pe-
122 riod. The Argo climatology exhibits a minimum salinity tongue in the central basin (at

123 25 °W; Figure 1c) extending from its formation region (between 45 and 60°S) across the
124 mixed layer to a maximum depth of 600–1200 m at 35–40°S. The salinity minimum follows
125 closely the depth of the isopycnal $\sigma_\theta = 27.2 \text{ Kg/m}^3$, which is approximately 1000 m deep
126 in this region. Previous studies have associated the depth of the salinity minimum with
127 the $\sigma_\theta = 27.2 \text{ Kg/m}^3$ isopycnal surface, and also with the neutral density surface $\gamma_n = 27.4$
128 Kg/m^3 [You, 2002]. North of 20 °S, the $\sigma_\theta = 27.2 \text{ Kg/m}^3$ density surface levels out to
129 a depth of 700 m, and the salinity minimum flows underneath a salty surface region of
130 maximum evaporation minus precipitation (E-P).

131 SODA shows features analogous to the observations over a similar period (i.e., 2004–
132 2009; Figure 1a). In SODA, the isopycnals south of 40°S are much more tilted than
133 observations, and the maximum depth of the $\sigma_\theta = 27.2 \text{ Kg/m}^3$ is approximately 1200 m
134 deep, 200 m deeper than the observations. The salinity minimum in the South Atlantic
135 is also deeper in SODA than in the observations. This causes a maximum anomaly of
136 salinity on 40°S of up to 0.6 psu at 500 m depth (Figure 1d). At $\sim 7^\circ\text{S}$, SODA shows a
137 strong near-surface upwelling region, characterized by an uplifting of the isopycnals. This
138 feature is not evident in the ARGO climatology. ECCO2 results show that the minimum
139 salinity is well constrained, with a maximum depth at approximately 800 m, and the
140 differences of salinity with depth are therefore much reduced ($< 0.2 \text{ psu}$) in comparison
141 to SODA (Figure 1e).

142 Next, we compare the regional features of the salinity minimum in the South Atlantic
143 between the reanalyses and Argo, doing so after interpolating all products to the Argo
144 resolution. The salinity minimum surface in the South Atlantic is shown in Figure 2.
145 SODA shows a stronger Subantarctic Front (STF; $\sim 45^\circ\text{S}$) than in observations (Figure

146 2a, c), which agrees with the larger isopycnal slopes in that region, as revealed in Figure
147 1a. For this reason the STF region shows the largest salinity differences (~ 0.3) between
148 SODA and Argo (Figure 2d). In the other regions salinity differences are smaller, and can
149 reach approximately 0.1 in magnitude. ECCO2 (Figure 2b) shows a better representation
150 of the STF region relative to SODA, and the biases are below 0.15 psu in the region.
151 North of 30°S , biases in ECCO2 and SODA show similar magnitudes. Although there
152 are differences within the two reanalysis products, which are based on different models,
153 assimilation methods and observations assimilated, and between the reanalysis products
154 and observations, similar results in terms of their temporal and spatial variability will
155 lend credence to the robustness of the variability of the AAIW in the region.

3.2. Regional trends in the AAIW

156 In the South Atlantic, changes in the relationship of temperature and salinity along
157 isopycnals show latitudinal dependence. The time and latitude distribution of the South
158 Atlantic salinity at various density levels from the 1960s to 2000s is here inferred from
159 Temperature-Salinity (θ/S) diagrams for four latitudes (35°S , 30°S , 20°S , 10°S ; Figure 3).

160 At 35°S (Figure 3a), SODA (solid lines) show strong salinity variability in the ther-
161 mocline waters. Salinity values are higher in the 2000s, although this increase is not
162 monotonic over time, instead alternating, with the 1970s and 1990s having lower salinity
163 values, and the 1960s, 1980s and 2000s having higher salinity values. Similar alternating
164 patterns are found along 30°S and 10°S (Figures 3b and 3d, respectively). At 10°S , which
165 is located in the tropical region of high E-P, salinity increases by 0.2 in the upper tropical
166 waters, which is related an enhanced hydrological cycle in the region [*Curry et al.*, 2003;
167 *Helm et al.*, 2010]. At 20°S (Figure 3c), the 2000s SODA shows lower salinity values at the

168 thermocline, and higher values in the 1970s. The smallest differences in θ/S over time are
169 found at 20°S for the whole profile. The central and intermediate water levels generally
170 have opposing signs of changes at all latitudes. Central waters show a recent cooling and
171 freshening along isopycnals, as is apparent in the density layer between $\sigma = 26.5$ and
172 27.0 kg m^{-3} , whereas intermediate waters generally show warming and increased salinity
173 between $\sigma = 27.2$ and 27.4 kg m^{-3} (highlighted in the insets of Figure 3). Central water
174 freshening has been suggested to be related to changes in subduction processes at this
175 density range [*Durack and Wijffels, 2010*]. ECCO2 (dashed lines) shows higher surface
176 salinities than SODA in the thermocline, specially at higher latitudes (Figures 3a, b),
177 and generally lower salinity values in intermediate levels. Salinity changes in ECCO2,
178 however, agree with SODA in that there is a salinity increase in the thermocline and
179 intermediate layers, and a decrease in the central water layers.

180 The spatial distribution of salinity minimum trends in SODA and ECCO2 are shown in
181 Figures (4a, b). For consistency, the trends are calculated since 1992 for the two products.
182 SODA and ECCO2 show an increase in the salinity minimum since 1992 almost everywhere
183 in the South Atlantic.

184 To investigate how the trends in the dynamical parameters at the salinity minimum
185 position observed in Figures (4a,b) are significant over time, we produce a time series
186 of the salinity, potential density (σ_θ) and temperature anomalies for SODA and ECCO2
187 relative to the SODA's average over its whole time series period at the depth of the salinity
188 minimum. We consider two locations in the central part of the basin, at 25°W/30°S and
189 25°W/35°S (Figure 4). At both latitudes, SODA (black line) shows an increase in salinity
190 and temperature in the late 1980s/beginning of 1990s until the end of the series (Figure

191 4c,g,d,h). This joint effect of warming and salinification produces a reduction in density
192 during this period (Figure 4e,f); a feature that agrees with climate projections of the
193 AAIW [*Goes et al.*, 2008]. The effect of the density decrease at the minimum salinity
194 depth is more prominent at 35°S than at 30°S. There is strong decadal variability at both
195 latitudes, although fluctuations appear in different periods: at 30°S, there is a general
196 freshening trend from the 1960s to the 1970s, and an increase in salinity after 1976 (Figure
197 4c). The rate of salinity increase from the mid-1970s to the mid-1990s is the highest with
198 about 0.01 per decade, while it levels out considerably in the late 1990s and 2000s.

199 At 35°S there is a significant positive salinity anomaly in the 1970s, followed by an also
200 significant negative salinity anomaly in the 1980s. A linear trend of about 0.05 per decade
201 is apparent after that. Trends observed in SODA after 2000 in all analyzed parameters
202 exceed 3 standard deviations (red dashed lines in Figure 4) calculated for the whole time
203 series period, showing that these trends are likely to be statistically significant. Timeseries
204 of ECCO2 (blue lines) for temperature, salinity and density show much stronger variability
205 than found SODA, which makes the detection of salinity changes since 1992 more difficult.
206 However, property changes in ECCO2 compares well with the ones from SODA for the
207 same period.

208 The interannual-to-decadal salinity changes shown in Figure (4) are consistent with re-
209 cent findings that changes in the rate of global surface temperature increase have occurred
210 in previous decades, such as in the mid-1970s [*Levinson and Lawrimore*, 2008; *Trenberth*
211 *and Coauthors*, 2007], and that these changes can potentially produce signals in density
212 and salinity at depth [*Durack and Wijffels*, 2010].

3.3. Density changes in the subtropical Atlantic

213 According to *Bindoff and McDougall* [1994], salinity changes at depth have three main
214 causes: i) freshening/salinification on isopycnals, ii) warming/cooling on isopycnals and
215 iii) heave, which is related to vertical displacements of isopycnals without changes in
216 salinity and temperature. Therefore, knowledge of these salinity changes requires under-
217 standing the causes of density changes at intermediate levels.

218 Timeseries in Figure 4 suggest that there is compensation between temperature and
219 salinity at the salinity minimum depth. An increase in salinity, which forces an increase
220 in density, is accompanied by an increase in temperature, and consequently a decrease in
221 density.

222 We investigate the causes of variability of density around the salinity minimum depth
223 (~ 1000 m) by estimating the thermopycnal and halopycnal changes at that depth. For
224 this we keep the salinity or temperature constant at their climatological mean values,
225 and let the other component vary over time. This way, we are able to estimate the main
226 contribution of density changes, which drive the large-scale meridional water displacement
227 in the ocean.

228 The correlation between the thermopycnal and halopycnal terms provide information
229 of the compensation between them (Figure 5). If the components are highly negatively
230 correlated, strong compensation is diagnosed. In opposition, weak or positive correlation
231 means that one of the terms is probably controlling the density changes. SODA and
232 ECCO2 show that there are dominant regions of compensation. Compensation occur
233 mostly in the middle of the subtropical gyre, where correlation between the thermal and
234 haline terms are often below -0.7 . In the regions that compensation happens, the individ-

235 ual components have weak correlation with density (not shown), therefore no contribution
236 is dominant. North of 30°S, the two components are positively correlated, and in this part
237 of the domain temperature is a stronger driver of density changes.

238 This compensating behavior can explain the larger variability of salinity values on isopy-
239 cnals at 35°S than at 30°S, shown in Figure 4. Other studies have found similar com-
240 pensating patterns in the North Atlantic [*Lozier et al.*, 2010], where compensation on
241 decadal timescales is associated with water mass changes, rather than heave mechanisms.
242 Since ECCO2 reanalysis only spans for two decades, which would hinder our ability to
243 meaningfully interpret its changes as a part of a longer-term trend, we use SODA 2.2.6
244 to infer how salinity and gyre changes are inter-related in the South Atlantic.

3.4. Subtropical Gyre variability in SODA

245 An AAIW layer, which encompasses the the salinity minimum surface depths (~ 800 –
246 1100 m), is constructed by defining two neutral density surfaces [*Jackett and McDougall*,
247 1997] as the upper and lower boundaries, the $\gamma_n = 27.1$ and $\gamma_n = 27.6$, respectively.
248 Within this layer (Figure 6a), there is a signature of the inflow of salty Indian Ocean
249 waters through the southeastern tip of the Atlantic. The high salinity Indian Ocean wa-
250 ters at intermediate levels are formed in the Red Sea [*Talley*, 2002], and flow into the
251 Agulhas Current through the Mozambique Channel. While entering the South Atlantic,
252 the mixing with the AAIW low salinity waters modify the Red Sea water along its tra-
253 jectory northwestward. The low salinity AAIW waters are originated in large extent in
254 the southeastern Pacific [*McCartney*, 1977; *Saenko et al.*, 2003] and flow eastward along
255 the sub-Antarctic front (SAF). The AAIW follows a path similar to the one predicted by
256 the ventilated thermocline theory [*Schmid et al.*, 2000], and a "shadow zone" is formed

257 in the northeast part of the South Atlantic, which also contains relatively high salinity
258 values. From Figure 6a, a minimum on the salinity minimum surface is obvious at about
259 30°S (Figure 6a), crossing the basin from east to west following the Benguela Current
260 Extension [*Schmid and Garzoli*, 2009], which feeds into the Brazil Current (BC) along
261 the western boundary. BC waters encounter the Malvinas Current waters between 35°S
262 and 40°S, resulting in a westward inflow of low salinity waters along the South Atlantic
263 Current [*Goni and Wainer*, 2001; *Wainer et al.*, 2000].

264 SODA shows decadal changes in salinity between the 1960 and 2000 (Figure 6b–e).
265 Compared to the 1960s, the 1970s and the 1980s show a slight decrease in the minimum
266 salinity in most parts of the South Atlantic. A noticeable feature in the 1970s and later
267 in the 1990s and 2000s is the southward shift of the Brazil-Malvinas confluence up to
268 approximately 3 degrees, in comparison to the 1960s. This shift produces positive salinity
269 anomalies north and negative south of 35°S in the western part of the basin. In opposition,
270 the 1980s (Figure 6c) show a northward migration of the confluence, which can explain
271 some of the decadal variability shown in Figures (4d,h).

272 The 1990s show reduced salinity in the center of the salinity minimum south of 35°S,
273 and a general increase of salinity in the rest of the basin. These changes agree with results
274 from *Schmidtke and Johnson* [2012], in that negative salinity trends are observed in this
275 region over the past 50 years, although these trends are not statistically significant.

276 Of great importance is the enhanced inflow of higher salinity waters from the Agulhas
277 Current retroflection region in the southeastern part of the basin, which increases the
278 signature of these waters toward the northwestern part of the basin. In the 2000s (Figure
279 6e), this positive salinity trend in the basin continues, and increased salinity values are also

280 found on the western side of the basin. This can have implications for the interhemispheric
281 transport through the North Brazil Undercurrent, as shown in [Bjastoch *et al.*, 2008].

Advective mechanisms within the gyre have the potential to drive a large part of the salinity increase displayed in SODA. This can be quantified with potential vorticity (PV) maps for the defined intermediate layer (Figure 7). The Ertel's PV is calculated as:

$$PV = \frac{f}{\rho_0} \frac{\Delta\gamma_n}{\Delta z} \quad (1)$$

282 where f is the Coriolis parameter, ρ_0 is the mean density of the ocean, and Δz is the layer
283 thickness.

284 The region is characterized by negative PV over the whole South Atlantic basin, char-
285 acteristic of the planetary vorticity of the region (Figure 7a). The anticyclonic subtropical
286 gyre is delimited by stronger negative vorticity ($PV < -6e^{-11}m^{-1}s^{-1}$). From Figure 7 we
287 can infer qualitatively the regions of high and low mixing. PV homogenization is generally
288 characteristic of high mixing, whereas across PV fronts there is inhibited mixing, since
289 they generate a barrier for the flow [Beal *et al.*, 2006]. The subtropical gyre is a natural
290 path for the flow to enter the basin, and high mixing occurs along its path westward
291 between 25-30°S.

292 The PV anomaly maps (Figure 7b-d) reveal that, starting in the 1980s, the PV in
293 the AAIW layer has become more negative within the subtropical gyre. This suggests a
294 spin-up of the anticyclonic gyre recently. Additionally, there has been an expansion of
295 the negative gyre's PV southward, in agreement with observational results suggesting an
296 expansion southward of the surface subtropical gyre [Roemmich *et al.*, 2007; Goni *et al.*,
297 2011], and a sectional poleward migration of the ACC [Gille, 2008]. This effect could
298 potentially increase the mixing between Agulhas and South Atlantic waters in the eastern

299 part of the basin. It would displace the minimum salinity region in the southwestern part
300 of the salinity minimum surface to the south, promoting the increase of salinity north of
301 this region.

302 The gyre strength and location are associated to the Sverdrup dynamics, therefore
303 determined by the strength and location of the wind stress curl, respectively. Some
304 properties of the wind stress in SODA are shown in Figure 8. Since 1960s there has been
305 an overall increase in the westerlies strength in the eastern side of the basin, from 0.13
306 Pa to 0.16 Pa in the 2000s (Figure 8a). This effect is accompanied by a slight southward
307 migration of the maximum wind stress curl (Figure 8b), from 38°S in the 1960s to 40°S
308 in the 2000s, and an increase in the maximum wind stress curl from 19 Pa/m to 26 Pa/m
309 (Figure 8c). In response to this forcing, according to the Sverdrup dynamics, there would
310 be an extension of the gyre southwards that follows the latitude of the wind stress curl,
311 and a spin up of the gyre, as a response to an increase in the wind stress curl. As we shall
312 see, the magnitude of the westerlies in the eastern side of the basin affects the Agulhas
313 leakage and the input of high salinity waters to the South Atlantic at intermediate levels.

3.5. Westward propagating Rossby Waves

314 As noted by *McCarthy et al.* [2012], salinity anomalies can be generated at intermediate
315 depths in the eastern side of the basin, and propagate westward with a second mode Rossby
316 wave speed. *McCarthy et al.* [2012] suggests that this can be an important mechanism to
317 explain the variability of the salinity minimum across the basin on interannual timescales.
318 In Figure 6, there is a clear extension of the subtropical gyre and increase in the Agulhas
319 leakage at intermediate depths.

320 The Agulhas leakage is well correlated with the strength of the westerlies [*Durgadoo*
321 *et al.*, 2013] in the eastern part of the Atlantic basin. Similarly to *Durgadoo et al.* [2013],
322 we define an index for the strength of the westerlies in the eastern part of the basin as
323 the average zonal wind stress within 35°S–65°S and 0°W–20°E.

324 To investigate how salinity anomalies originated in the Agulhas leakage region are forced
325 by the westerly winds and spread over the South Atlantic, we apply to SODA a lagged
326 correlation of the westerly wind stress index in the eastern side of the basin to the salin-
327 ity minimum surface. The time series are previously smoothed with a 9-month Boxcar
328 window to filter the seasonal variability. The spatial distribution of the maximum lagged
329 correlations and their associated lags are shown in Figure 9. The lag of the maximum
330 correlation over space shows the propagation patterns of the salinity anomalies. Small
331 lag values, close to zero or even negative, are observed in the eastern side of the basin.
332 Negative lag values in the southeastern tip of the basin suggest that the flow in the Ag-
333 ulhas leakage is driven in great part by the wind stress anomalies east of Africa. Where
334 the lag shows smaller values, the correlation of the westerlies and the salinity anomalies
335 is highest, above 0.6. Anomalies propagate along a northwestern trajectory, following the
336 ocean circulation at that depth (Figure 7a). This is also a characteristic pattern of the
337 Rossby wave signal, which phase speed decreases poleward. The largest extension of the
338 westward propagation of the salinity anomalies is observed along 29°S, which exhibits a
339 time lag of approximately 120 months (10 years) to be completed. South of 30°S the lag
340 increases considerably up to 200 months, i.e., about 17 years.

341 To investigate whether Rossby wave propagation is a plausible dynamical mechanism
342 for the variability of the AAIW on interannual to decadal timescales, we examine time-

343 longitude plots (Hovmoller diagrams) at two latitudes, 30°S and 35°S (Figure 10). Hov-
344 moller diagrams allow us to determine zonal propagation patterns along a given latitude.
345 In these diagrams, propagating waves appear as diagonal bands across the basin, and
346 the slopes of these patterns are equal to the phase speed (c_p) of the waves. Here, wave
347 characteristics are assessed objectively using the Radon Transform (RT) applied to the
348 Hovmoller diagrams [*Challenor et al.*, 2001; *Polito and Liu*, 2003; *Barron et al.*, 2009].
349 This method rotates the coordinate system of the zonal-temporal diagrams in order to
350 find the patterns that best align with the rotated axis.

351 The Hovmoller diagrams are for salinity anomalies (calculated with respect to the an-
352 nual mean climatology) projected onto the $\gamma_n = 27.4$ neutral surface. Zonal means are
353 subtracted from the anomalies field to filter decadal trends [*Barron et al.*, 2009], thus
354 highlighting the interannual timescales. West-to-east propagating anomalies spread along
355 30°S. The optimal propagation speed is $cp = 1.79 \pm 0.48$ cm s⁻¹, at which anomalies
356 travel across the basin in approximately 10 years. A similar result is obtained in the lag
357 correlation maps shown in Figure 9. These speeds strongly agree with those obtained by
358 *McCarthy et al.* [2012], who estimated a propagation speed of $cp = 1.7$ cm s⁻¹, which is
359 characteristic of a second baroclinic mode wave propagation.

360 At 35°S, the situation is different. Propagation speeds of 0.47 ± 0.06 cm s⁻¹ are much
361 slower than the one predicted by the Rossby wave theory. In fact, the pattern of the
362 variability in the eastern part of the basin (east of 15°W) seems to be unrelated to the
363 one further west. From Figure 9, we observe that the correlations decrease considerably
364 from east to west at this latitude, and also the ability of the waters from the east to
365 mix westward. Figure 7a shows that there is a strong gradient of PV around 35°S and

366 15°W, the approximate position of the change in the propagation pattern shown in Figure
367 10b. According to *Beal et al.* [2006], PV fronts are able to prevent mixing and advection
368 along water masses trajectories. This effect may explain the low correlations of salinity
369 anomalies in the western part of the basin at this latitude, and regional dynamics should
370 play a larger role in this area.

371 To be assured, we performed additional calculations of the salinity propagation speeds
372 using ECCO2 at the 30°S and 35°S. The values found for ECCO2 are 1.84 ± 0.45 and 0.46
373 ± 0.1 m/s, respectively, in large agreement with the speeds retrieved for SODA, showing
374 that these results are robust across products.

3.6. Wind x CO₂

375 In the previous sections we show that SODA 2.2.6 exhibits changes in the subsurface
376 salinity minimum and circulation patterns at intermediate layers. These changes include
377 decadal variability overlapping a background low frequency variability, which becomes
378 stronger after the 1970s. Other studies confirm that similar subsurface changes have
379 occurred since 1950 [e.g., *Levitus et al.*, 2000; *Gille*, 2002; *Levitus et al.*, 2005; *Domingues*
380 *et al.*, 2008; *Levitus et al.*, 2009; *Durack and Wijffels*, 2010; *Gille*, 2008; *Lyman et al.*,
381 2010].

382 In order to examine the possible causes of the salinity minimum variability, we perform
383 idealized experiments with an Earth System Model of Intermediate Complexity in which
384 two possible forcings, the wind stress curl changes in the Atlantic and the global warming
385 due to CO₂ are separated. In these experiments, we use the University of Victoria Earth
386 System Model of Intermediate Complexity (UVic 2.9) [*Weaver et al.*, 2001]. This model
387 has been widely used in climate simulations and model comparison studies. We separate

388 the influences of the wind stress on the advective mechanisms in the South Atlantic into
389 northern and southern hemispheric forcings, by defining the first hemispheric modes of
390 variability, which are related to the North Atlantic Oscillation (NAO) and SAM, to the
391 north and south respectively. A description of the model experiments can be found in
392 Appendix A.

393 **3.6.1. AAIW changes in the intermediate complexity model**

394 Here, we analyze the response of the Atlantic salinity minimum surface to separate
395 atmospheric forcing, as described in Appendix A. Although UVic has a coarse resolution,
396 it can represent the salinity minimum surface below 200 m depth reasonably well (Figure
397 11a). The effect of different forcings on the recent (2000s) anomalies in the salinity
398 minimum are separated by subtracting hierarchically a forced simulation from another
399 simulation without that forcing. Salinity minimum changes in the UVic model (Figures
400 11b–d) are heterogeneous over the spatial domain (Figure 11). This feature agrees with
401 those features observed in SODA (Figure 6).

402 Adding SAM as a forcing mechanism (Figure 11b) produces mostly positive salinity
403 anomalies in the South Atlantic, and some negative anomalies in the Indian Ocean sector,
404 predominantly within the mixed layer. Anomalies forced by SAM are mostly driven by a
405 strengthening and displacement the westerlies southward.

406 Anomalies generated by a historical NAO-like pattern (Figure 11c) are much weaker
407 with respect to those generated with SAM or CO₂ forcings, and show mostly negative
408 salinity anomalies within the subtropical gyre. Forcing due to increased CO₂ concentration
409 in the 2000s (Figure 11d) produces a salinity increase in the subtropical South Atlantic,
410 and negative anomalies in shallower waters along the South Atlantic Current and ACC.

411 The South Atlantic salinity response to CO₂ is similar but weaker than the response forced
412 by SAM. This result is not what is expect considering the freshening that occurs in the
413 Southern Ocean under global warming due to increased precipitation, as shown by the
414 large negative anomalies south of 40°S. The analysis of zonal averaged salinity anomalies
415 along isopycnals, remapped on depth levels (Figure 12b), show that the freshening and
416 warming in the Southern Ocean produce positive salinity anomalies on isopycnals, and
417 this signal is spread northward along the salinity minimum surface. Slightly above the
418 salinity minimum, there is freshening on isopycnals, which is consistent with previous
419 works [*Curry et al.*, 2003; *Durack and Wijffels*, 2010; *Bindoff and Coauthors*, 2007]. Both
420 salinification along isopycnals in the Southern Ocean and in the core of the AAIW, as
421 well as the freshening above the core of the AAIW are consistent with the shoaling of
422 the isopycnals and increased stratification driven by surface warming, in agreement with
423 [*Schmidtko and Johnson*, 2012]. The SAM effect on salinity on isopycnals is somewhat
424 opposite to CO₂, with salinification on the upper part of the AAIW, and freshening below
425 the salinity minimum, and south of 50°S.

426 The time series of salinity and temperature at the location of the salinity minimum
427 at 30°S/25°W for the UVic model are shown in Figure 13. The CONTROL simulation,
428 without transient forcing (red curve), shows a salinity of ~ 34.57 and temperature of
429 ~ 4.39 °C at the salinity minimum depth from 1870 to 2009. Salinity changes, relative
430 to the CONTROL simulation, that are driven by wind changes in response to the SAM
431 atmospheric pressure forcing (green curve in Figure 13a) are negative from 1870 to 1950
432 in the model. Changes in the SAM phase after the 1960s strengthen and displace the
433 westerlies southward, driving positive salinity anomalies that are modulated by decadal

434 variability. In 2008, the salinity is 0.015 above the pre-industrial level. When a NAO-like
435 forcing is considered in addition to the SAM forcing (blue curve in Figure 13), additional
436 changes are minor, and the trends due to wind variability do not differ from the SAM-only
437 experiment. Finally, when CO₂ forcing is added on the top of SAM and NAO forcings
438 (turquoise curve in Figure 13), there is an increase in the positive trend in the salinity
439 minimum after 1950 in comparison to the SAM-only experiment. This trend driven by
440 the CO₂, load in the atmosphere is strongly linear. The 2008 salinity anomaly relative to
441 the pre-industrial values is 0.025 psu. Therefore, the CO₂ indirect forcing through wind
442 changes is responsible for 50% of the simulated AAIW salinity anomalies due to SAM in
443 the 2000s.

444 Although secondary in driving historical salinity anomalies in the AAIW, CO₂ forcing
445 is the main contributor for the increase in temperature anomalies at the depth of the
446 salinity minimum (Figure 13b). While SAM-like forcing accounts for 0.1°C relative to the
447 CONTROL run, adding the CO₂ forcing has a direct effect to increase the temperature
448 anomalies to 0.3°C, a contribution of 2/3 of the recent warming of the AAIW, while SAM
449 accounts for just 1/3. The NAO-like forcing is again a minor contribution to the AAIW
450 variability in the South Atlantic.

4. Discussion

451 Many physical processes can cause changes in the South Atlantic variability in partic-
452 ular, and in the Southern Hemisphere climate in general. These range from greenhouse
453 gases concentrations in the atmosphere (CO₂), to the major modes of coupled variability.
454 These atmospheric patterns can cause non-monotonic interdecadal fluctuations in the θ/S
455 relationships at depth, as revealed in previous studies [e.g., *Garabato et al.*, 2009].

5. Discussion and Conclusions

456 By investigating the decadal changes in the minimum salinity layer for the subtropical
457 South Atlantic, we have established the relationship between density changes with large
458 scale climate trends. We used outputs from a reanalysis products, SODA 2.2.6, to verify
459 the changes in the salinity minimum from 1960s. The changes in more recent years
460 (starting in 1992) are compared to another reanalysis, ECCO2. The two products produce
461 different climatologies of salinity minimum in the 2000s, and ECCO2 shows less bias
462 towards observations, since it assimilates both surface and profiles data. In SODA, the
463 AAIW core reaches depths of 1200 m, in comparison to 800m for Argo observations
464 and ECCO2. Therefore, SODA shows stronger isopycnal slopes around the outcropping
465 region of the AAIW in the South Atlantic (45° – 50° S), and the salinity minimum signature
466 in depth spreads unsullied further north than observations and ECCO2. Both processes
467 suggest weak isopycnal mixing in SODA. The slope of the isopycnals in the Southern Ocean
468 is mostly set by the westerly winds strength, and partly compensated by an opposing
469 eddy-induced circulation, which is mostly directed along isopycnals [*Marshall and Radko,*
470 *2003; Obers and Visbeck, 2005; Meredith et. al , 2012, e.g.,*]. This feature is generally
471 parameterized in climate models using the Gent and McWilliams [1990] scheme. Even
472 though the climatology of the AAIW differ, the two reanalysis agree well in terms of
473 the variability in the last two decades. Significant trends are observed in SODA and
474 ECCO2 since the late 1990s in salinity, temperature and density at intermediate levels.
475 We found a latitudinal dependence on the contribution of temperature and salinity to
476 density changes that would ultimately drive the meridional water displacement in the
477 ocean. South of 30° S, and within the subtropical gyre, there is strong compensation

478 between salinity and temperature, which may drive larger trends in those fields because
479 of the dynamical influence of salinity. North of 30°S, salinity and temperature changes
480 are positively correlated, and temperature dominates the density changes.

481 In SODA, we determined two main dynamic factors for the salinity increase in the
482 South Atlantic salinity minimum region: i) the expansion and spin up of the subtropical
483 gyre, driven by enhanced wind stress curl and a shift southward, increases mixing of high
484 salinity Agulhas leakage waters into the South Atlantic; and ii) the strengthening of the
485 westerlies forces an increase in the Agulhas leakage, and, therefore, the input of high
486 salinity waters at intermediate depths into the South Atlantic.

487 Different dynamic mechanisms are also present at different latitudes which determine
488 the spread of the high salinity waters from the southeast boundary into the Atlantic.
489 Our results show that the strengthening of the westerlies are positively correlated with
490 the salinity minimum anomalies in most part the basin. At 30°S, the salinity anomalies
491 generated by increased westerlies in the southeastern Atlantic follow a path defined by
492 the Benguela Current and the Benguela Current Extension, in which changes in salinity
493 at this latitude are highly driven by ocean adjustment through a second mode Rossby
494 wave mechanism. This result is in agreement with previous studies [e.g., *McCarthy et al.*,
495 2012; *Durgadoo et al.*, 2013], and in both SODA and ECCO2 reanalysis. Therefore, the
496 reported present-day leakage increase could reflect an unadjusted oceanic response mainly
497 to the strengthening westerlies over the last few decades.

498 At 35°S, there is a discontinuity in the propagation pattern at approximately 15°W,
499 and the propagation speeds of the westward salinity anomalies, revealed by the method
500 applied here, are much slower than what linear wave theory predicts. Previous studies

501 have shown that bathymetric features, such as the Mid-Atlantic Ridge can discontinue
502 the propagation of Rossby waves [*Vianna and Menezes*, 2013]. This does not seem to be
503 the case here, since at 35°S the steepest part of the Ridge is located at approximately
504 0°W. Instead, a PV front at that latitude prevents the spread of the anomalies westward
505 reducing the mixing of high salinity anomalies from the Agulhas leakage region, similar to
506 the effect described in [*Beal et al.*, 2006]. The lags of the maximum correlation show that
507 salinity anomalies take up to 17 years to cross basin since they are forced in the eastern
508 side. The southwestern side of the basin, near the Brazil-Malvinas Confluence, show
509 negative and not statistically significant correlations with salinity minimum anomalies in
510 the southwestern part of the basin. This result corroborate to our above mentioned results
511 showing that salinity anomalies cannot freely propagate westward at those latitudes, and,
512 therefore, at those locations other processes may be determine the regional variability of
513 salinity. In fact, as described in *Schmidtke and Johnson* [2012], the southwestern region
514 of the South Atlantic shows a negative and not significant salinity trend at intermediate
515 levels, in opposition with the positive salinity decadal trend in most of the South Atlantic.

516 The sensitivity studies with the UVic2.9 model indicate that the SAM is the predomi-
517 nant forcing of salinity changes in the sub-surface South Atlantic when compared to the
518 NAO and CO₂ forcing. The positive trend in SAM is associated with cooling at high
519 southern latitudes and strengthening of the latitudinal temperature gradient, leading to
520 stronger subtropical and westerly winds, and a southward displacement of the westerlies
521 [*Hall and Visbeck*, 2002; *Silvestri and Vera*, 2003; *Lefebvre et al.*, 2004; *Sen Gupta and*
522 *England*, 2006; *Gillett et al.*, 2006; *Toggweiler et al.*, 2009; *Thompson et al.*, 2011]. The
523 strengthening and Southward displacement of the westerlies increase the Agulhas leakage

524 [*Durgadoo et al.*, 2013], in a mechanism that must be unrelated to the model resolution.
525 NAO variability, which largely affects the water masses properties in the the North At-
526 lantic [*Arbic and Brechner Owens*, 2001], and the water mass formation of the Labrador
527 Sea and Greenland Sea water, does not seem to affect the spread of the salinity minimum
528 in the South Atlantic. This result can have implications for paleoclimate studies, which
529 relate the water mass formation in both hemispheres as a potentially coupled system
530 [*Wainer et al.*, 2012].

531 Warming due to CO₂ loading increases precipitation relatively to evaporation in the
532 Southern Ocean [*Curry et al.*, 2003; *Held and Soden*, 2006; *Durack and Wijffels*, 2010;
533 *Helm et al.*, 2010], producing a surface freshening of the ocean [*Boyer et al.*, 2005; *Boning*
534 *et al.*, 2008]. Although this region encompasses the formation regions of the AAIW, our
535 experiments show a salinity increase along isopycnal in the Southern Ocean and in the
536 salinity minimum surface due to CO₂. Our results suggest that the strong warming and
537 freshening that happens south of 45°S decrease the density and shoals the isopycnals, in
538 agreement with [*Schmidtko and Johnson*, 2012].

539 *Bindoff and McDougall* [1994] analyze salinity and temperature changes in isopycnals
540 as pure heating, pure freshening and heave. More recent studies call attention to the
541 lateral advection of these properties along isopycnals, and therefore, circulation changes
542 would be a source of salinity changes on isopycnals [*Durack and Wijffels*, 2010; *Schmidtko*
543 *and Johnson*, 2012]. Here we confirm the role of lateral advection in increasing leakage of
544 salty Agulhas waters at intermediate levels, driven by the large-scale wind variability in
545 the region.

Appendix A: The climate model of intermediate complexity

546 In the present work we use the latest version of the University of Victoria Earth System
547 Model (UVic 2.9). The ocean component of UVic 2.9 [Weaver *et al.*, 2001] is MOM2
548 [Pacanowski, 1995] with a $1.8^\circ \times 3.6^\circ$ resolution in the horizontal and 19 depth levels.
549 Diapycnal diffusivity is parameterized as $K_v = K_{tidal} + K_{bg}$, which consists of the mixing
550 due to local dissipation of tidal energy (K_{tidal}) [Laurent *et al.*, 2002; Simmons *et al.*, 2004]
551 plus a background diffusivity $K_{bg} = 0.3 \text{ cm}^2 \text{ s}^{-1}$. The atmospheric component is a one-
552 layer atmospheric energy-moisture balance model, which does not apply flux correction
553 and is forced by prescribed winds from the NCEP/NCAR climatology. Also included in
554 the model are a thermodynamic sea ice component, a terrestrial vegetation (TRIFFID),
555 and an oceanic biogeochemistry based on the ecosystem model of [Schmittner, 2005]. The
556 model is spun up for 3000 years, and then four experiments are performed (Table 1).
557 First, the CONTROL experiment is a non-transient experiment forced with atmospheric
558 forcings from the 1800 levels. The second to fourth experiments use, in addition to the
559 NCEP/NCAR wind stress climatology, wind stress anomalies calculated from the first
560 empirical mode (EOF1) of sea level pressure (SLP) anomalies in the northern and southern
561 hemispheres (Figure 14). These modes are a good approximation of the North Atlantic
562 Oscillation (NAO), in which the positive phase is characterized by low SLP anomalies
563 over Iceland and high SLP anomalies over the Azores, and the Southern Annular Mode
564 (SAM), which is characterized by low SLP anomalies over Antarctica, respectively. More
565 specifically, the second experiment uses the SAM EOF forcing only, the third experiment
566 uses the NAO EOF forcing only, and the fourth experiment uses both the SAM and the
567 NAO forcings plus historical global CO_2 emissions, under which the atmospheric CO_2

568 concentration levels reach 384 ppmV in 2009. The hemispheric SLP modes are calculated
569 from the *Compo et al.* [2006] dataset and start in the year 1871. When the SLP anomalies
570 related to the hemispheric modes of variability are added to the model, the associated
571 wind stress anomalies are calculated using a frictional geostrophic approximation [*Weaver*
572 *et al.*, 2001]. In addition to the SLP anomalies added to the climatological wind field,
573 wind stress anomalies can be further produced as a linear dynamic coupling to SAT
574 anomalies [*Weaver et al.*, 2001]. In UVic, the wind stress is converted to wind speed for
575 the calculation of the latent and sensible heat fluxes from the ocean [*Fanning and Weaver*,
576 1998]. All experiments are run from 1800–2008, keeping the other atmospheric forcings
577 (e.g., sulphate and volcanic aerosols) at the 1800 level.

578 **Acknowledgments.** This work is supported in part by NOAA/AOML and NOAA’s
579 Climate Program Office, and by grants from CAPES-ciencias-do-mar, 2013/02111-4 of the
580 São Paulo Research Foundation (FAPESP), CNPq-300223/93-5 and CNPq-MCT-INCT-
581 Criosfera 573720/2008-8.

References

- 582 Arbic, B. K., and W. Brechner Owens (2001), Climatic Warming of Atlantic Intermediate
583 Waters*, *J. Climate*, *14*, 4091–4108.
- 584 Barron, C. N., A. B. Kara, and G. A. Jacobs (2009), Objective estimates of westward
585 rossby wave and eddy propagation from sea surface height analyses, *J. Geophys. Res.*,
586 *114*, C03,013.
- 587 Beal, L. M., Chereskin, T. K., Y. D. Lenn, and S. Elipot (2006), The Sources and Mixing
588 Characteristics of the Agulhas Current, *J. Phys. Oceanog.*, *36*, 2060–2074.

589 Biastoch, A., C. W. Böning, and J. R. E. Lutjeharms (2008), Agulhas leakage dynamics
590 affects decadal variability in Atlantic overturning circulation, *Nature*, *456*, 489–492.

591 Bindoff, N. L., and T. J. McDougall (1994), Diagnosing climate change and ocean venti-
592 lation using hydrographic data, *J. Phys. Oceanogr*, *24*, 1137–1152.

593 Bindoff, N. L., and Coauthors (2007), Observations: Oceanic climate change and sea level.
594 *Climate Change 2007: The Physical Science Basis*, S. Solomon et al., Eds., Cambridge
595 University Press, 385–432.

596 Böning, C. W., A. Dispert, S. M. Visbeck, R. Rintoul, and F. U. Schwarzkopf (2008),
597 The response of the Antarctic Circumpolar Current to recent climate change, *Nature*
598 *Geosci.*, *1*, 864–869.

599 Boyer, T., S. Levitus, J. Antonov, R. Locarnini, and H. Garcia (2005), Linear trends in
600 salinity for the world ocean, 1955–1998, *Geophys. Res. Lett.*, *32*(1), 1–4.

601 Carton, J., and B. Giese (2008), A reanalysis of ocean climate using simple ocean data
602 assimilation (SODA), *Mon. Weath. Rev.*, *136*(8), 2999–3017.

603 Challenor, P. G., P. Cipollini, and D. Cromwell (2001), Use of the 3D radon transform
604 to examine the properties of oceanic Rossby waves, *J. Atmos. Oceanic Technol.*, *18*,
605 1558–1566.

606 Compo, G., J. Whitaker, and P. Sardeshmukh (2006), Feasibility of a 100-year reanalysis
607 using only surface pressure data, *Bull. Amer. Meteor. Soc.*, *87*, 175–190.

608 Compo, G., J. Whitaker, P. Sardeshmukh, N. Matsui, R. Allan, X. Yin, B. Gleason,
609 R. Vose, G. Rutledge, P. Bessemoulin, et al. (2011), The twentieth century reanalysis
610 project, *Quart. Jour. Royal Met. Soc.*, *137*(654), 1–28.

611 Curry, R., B. Dickson, I. Yashayaev, et al. (2003), A change in the freshwater balance of
612 the atlantic ocean over the past four decades, *Nature*, *426*(6968), 826–829.

613 Domingues, C. M., J. A. Church, N. J. White, P. J. Gleckler, S. E. Wijffels, P. M. Barker,
614 and J. R. Dunn (2008), Improved estimates of upper-ocean warming and multi-decadal
615 sea-level rise, *Nature*, *453*(7198), 1090–1093.

616 Durack, P., and S. Wijffels (2010), Fifty-year trends in global ocean salinities and their
617 relationship to broad-scale warming, *J. Climate*, *23*(16), 4342–4362.

618 Durgadoo, J. V., B. R. Loveday, C. J. C. Reason, P. Penven, and A. Biastoch (2013),
619 Agulhas leakage predominantly responds to the Southern Hemisphere westerlies, *J.*
620 *Phys. Oceanogr.*, *43*, 2113–2131.

621 Fanning, A. F., and A. J. Weaver (1998), Thermohaline variability: The effects of hori-
622 zontal resolution and diffusion, *J. Climate*, *11*(4), 709–715.

623 Garabato, A. C. N., L. Jullion, D. P. Stevens, K. J. Heywood, and B. A. King (2009),
624 Variability of subantarctic mode water and antarctic intermediate water in the drake
625 passage during the late-twentieth and early-twenty-first centuries, *J. Climate*, *22*(13),
626 3661–3688.

627 Gent, P. R., and J. C. McWilliams (1990), Isopycnal mixing in ocean circulation models, *J.*
628 *Phys. Oceanogr.*, *20*, 150–155.

629 Gille, S. (2008), Decadal-scale temperature trends in the Southern Hemisphere ocean, *J.*
630 *Climate*, *21*, 4749–4765.

631 Gille, S. T. (2002), Warming of the southern ocean since the 1950s, *Science*, *295*, 1275–
632 1277.

633 Gillett, N., T. Kell, and P. Jones (2006), Regional climate impacts of the Southern Annular
634 Mode, *Geophys. Res. Lett.*, *33*(23).

635 Goes, M., I. Wainer, P. R. Gent, and F. O. Bryan (2008), Changes in subduction in the
636 South Atlantic Ocean during the 21st century in the CCSM3, *Geophys. Res. Lett.*, *35*,
637 6701–+.

638 Goni, G. J. and Wainer, I. (2001), Investigation of the Brazil Current front variability
639 from altimeter data, *J. Geophys. Res.*, *106*(C12), 31117–31128.

640 Goni, G. J., F. Bringas, and P. N. DiNezio (2011), Observed low frequency variability of
641 the Brazil Current front, *J. Geophys. Res. – Oceans*, *116*(C10037).

642 Grodsky, S., J. Carton, and F. Bingham (2006), Low frequency variation of sea surface
643 salinity in the tropical Atlantic, *Geophys. Res. Lett.*, *33*(14), L14,604.

644 Hall, A., and M. Visbeck (2002), Synchronous variability in the Southern Hemisphere
645 atmosphere, sea ice, and ocean resulting from the annular mode*, *J. Climate*, *15*(21),
646 3043–3057.

647 Held, I. M., and B. J. Soden (2006), Robust Responses of the Hydrological Cycle to Global
648 Warming, *J. Climate*, *19*, 5686–5699.

649 Helm, K. P., N. L. Bindoff, and J. A. Church (2010), Changes in the global hydrological-
650 cycle inferred from ocean salinity, *Geophys. Res. Lett.*, *37*, L18701.

651 Jackett, D. R., and T. J. McDougall (1997), A neutral density variable for the worlds
652 oceans, *J. Phys. Oceanogr.*, *27*, 237–263.

653 Laurent, L. S., H. Simmons, and S. Jayne (2002), Estimating tidally driven mixing in the
654 deep ocean, *Geophys. Res. Lett.*, *29*(23), 2106.

655 Lefebvre, W., H. Goosse, R. Timmermann, and T. Fichefet (2004), Influence of the South-
656 ern Annular Mode on the sea ice–ocean system, *J. Geophys. Res.: Oceans*, *109*(C9).

657 Levinson, D. H., and J. H. Lawrimore (2008), State of the climate in 2007, *Bull. Amer.*
658 *Meteor. Soc.*, *89*, S1–S179.

659 Levitus, S., J. Antonov, T. Boyer, and C. Stephens (2000), Warming of the world ocean,
660 *Science*, *287*, 2225–2229.

661 Levitus, S., J. I. Antonov, and T. P. Boyer (2005), Warming of the world ocean, 1955–2003,
662 *Geophys. Res. Lett.*, *32*, L02,604.

663 Levitus, S., J. Antonov, T. Boyer, R. Locarnini, H. Garcia, and A. Mishonov (2009),
664 Global ocean heat content 1955–2008 in light of recently revealed instrumentation prob-
665 lems, *Geophys. Res. Lett.*, *36*(7).

666 Lozier, M. S., V. Roussenov, M. S. C. Reed, and R. G. Williams (2010), Opposing decadal
667 changes for the North Atlantic meridional overturning circulation. *Nature Geosc.*, *3*,
668 728–734.

669 Lyman, J. M., S. A. Good, V. V. Gouretski, M. Ishii, G. C. Johnson, M. D. Palmer,
670 D. M. Smith, and J. K. Willis (2010), Robust warming of the global upper ocean,
671 *Nature*, *465*(7296), 334–337.

672 Marshall, J., A. Adcroft, C. Hill, L. Perelman, and C. Heisey (1997), A finite-volume,
673 incompressible Navier Stokes model for studies of the ocean on parallel computers, *J.*
674 *Geophys. Res.*, *102*(C3), 5753–5766.

675 Marshall, J., and T. Radko (2003), Residual-Mean Solutions for the Antarctic Circumpolar
676 Current and Its Associated Overturning Circulation, *J. Phys. Ocean.*, *33*, 2341–2354.

677 McCarthy, G., E. McDonagh, and B. King (2011), Decadal Variability of Thermocline and
678 Intermediate Waters at 24°S in the South Atlantic, *J. Phys. Oceanogr.*, *41*, 157–165.

679 McCarthy, G. D., B. A. King, P. Cipollini, E. L. McDonagh, J. R. Blundell, and A. Bi-
680 astoch (2012), On the sub-decadal variability of South Atlantic Antarctic Intermediate
681 Water, *Geophys. Res. Lett.*, *39*, L10,605.

682 McCartney, M. S. (1977), Subantarctic Mode Water. *A Voyage of Discovery*, M. V. Angel,
683 Ed., Pergamon, 103–119.

684 D. Menemenlis, I. Fukumori, and T. Lee (2005), Using Green’s functions to calibrate an
685 ocean general circulation model. *Mon. Weather Rev.*, *133*, 1224–1240.

686 D. Menemenlis, J. Campin, P. Heimbach, C. Hill, T. Lee, A. Nguyen, M. Schodlok, and
687 H. Zhang (2008), ECCO2: High resolution global ocean and sea ice data synthesis.
688 *Mercator Oce. Quart. Newsl.*, *31*, 13–21.

689 Meredith, M. E., A. C. Naveira Garabato, A. McC. Hogg, and R. Farneti (2012), Sen-
690 sitivity of the Overturning Circulation in the Southern Ocean to Decadal Changes in
691 Wind Forcing, *J. Climate*, *25*, 99–110.

692 Olbers, D., and M. Visbeck (2005), A model of the zonally averaged stratification and
693 overturning in the Southern Ocean, *J. Phys. Oceanogr.*, 1190–1205.

694 Onogi, K., J. Tsutsui, H. Koide, M. Sakamoto, S. Kobayashi, H. Hatsushika, T. Mat-
695 sumoto, N. Yamazaki, H. Kamahori, K. Takahashi, S. Kadokura, K. Wada, K. Kato, R.
696 Oyama, T. Ose, N. Mannoji, and R. Taira (2007), The JRA-25 Reanalysis, *J. Meteor.*
697 *Soc. Japan*, *85*, 369–432.

698 Pacanowski, R. (1995), MOM 2 documentation user’s guide and reference manual, GFDL
699 Ocean Group Technical Report No.3, *Fluid Dyn. Lab. NOAA, Princeton, NJ*.

700 Weijer, W., W. P. M. de Ruijter, A. Sterl, and S. S. Drijfhout (2002), Response of the
701 Atlantic overturning circulation to South Atlantic sources of buoyancy, *Global Planet.*
702 *Change*, *34*, 293–311.

703 Peeters, F. J. C., R. Acheson, G.-J. A. Brummer, W. P. M. de Ruijter, G. M. Ganssen,
704 R. R. Schneider, E. Ufkes, and D. Kroon (2004), Vigorous exchange between Indian
705 and Atlantic Ocean at the end of the last five glacial periods, *Nature*, *430*, 661–665.

706 Pierce, D. W., P. J. Gleckler, T. P. Barnett, B. D. Santer, and P. J. Durack (2012), The
707 fingerprint of human-induced changes in the oceans salinity and temperature fields,
708 *Geophys. Res. Lett.*, *39*, L21,704.

709 Polito, P. S., and W. T. Liu (2003), Global characterization of Rossby waves at several
710 spectral bands, *J. Geophys. Res.*, *108*.

711 Ray, S., and B. S. Giese (2012), Historical changes in El Niño and La Niña characteristics
712 in an ocean reanalysis, *J. Geophys. Res.*, *117*, C11,007.

713 Roemmich, D., and J. Gilson (2009), The 2004-2008 mean and annual cycle of temper-
714 ature, salinity, and steric height in the global ocean from the Argo program, *Progr.*
715 *Oceanogr.*, *82*, 81–100.

716 Roemmich, D., J. Gilson, R. Davis, P. Sutton, S. Wijffels, and S. Riser (2007), Decadal
717 spinup of the South Pacific subtropical gyre, *J. Phys. Oceanogr.*, *37*, 162–173.

718 Saenko, O. A., A. J. Weaver, and M. H. England (2003), A region of enhanced northward
719 Antarctic Intermediate Water transport in a coupled climate model, *J. Phys. Oceanogr.*,
720 *33*, 1528–1535.

721 Saenko, O. A., John C. Fyfe, and M. H. England (2005), On the response of the oceanic
722 wind-driven circulation to atmospheric CO₂ increase, *Clim. Dyn.*, *25*, 415–426.

723 Schmid, C., G. Siedler, and W. Zenk (2000), Dynamics of Intermediate Water circulation
724 in the subtropical South Atlantic, *J. Phys. Oceanogr.*, *30*, 3191–3211.

725 Schmid, C., and S. L. Garzoli (2009), New observations of the spreading and variability
726 of the Antarctic Intermediate Water in the Atlantic, *J. Marine Res.*, *67*(6), 815–843.

727 Schmidtko, S., and G. Johnson (2012), Multidecadal warming and shoaling of Antarctic
728 Intermediate Water*, *J. Climate*, *25*, 207–221.

729 Schmittner, A. (2005), Decline of the marine ecosystem caused by a reduction in the
730 Atlantic overturning circulation, *Nature*, *434*(7033), 628–633.

731 Sen Gupta, A., and M. H. England (2006), Coupled ocean-atmosphere-ice response to
732 variations in the Southern Annular Mode, *J. Climate*, *19*(18), 4457–4486.

733 Silvestri, G. E., and C. S. Vera (2003), Antarctic oscillation signal on precipitation anoma-
734 lies over southeastern South America, *Geophys. Res. Lett.*, *30*(21), 2115.

735 Simmons, H. L., S. R. Jayne, L. C. S. Laurent, and A. J. Weaver (2004), Tidally driven
736 mixing in a numerical model of the ocean general circulation, *Ocean Modell.*, *6*(3),
737 245–263.

738 Smith, R., J. Dukowicz, and R. Malone (1992), Parallel ocean general circulation model-
739 ing, *Physica D: Nonlinear Phenomena*, *60*(1), 38–61.

740 Talley, L. D. (2002), *Salinity patterns*, 11 pp., Encyclopedia of Global Environmental
741 Change, vol. 1, M. C. MacCracken and J. S. Perry, editors, John Wiley and Sons.

742 Thompson, D. W., S. Solomon, P. J. Kushner, M. H. England, K. M. Grise, and D. J.
743 Karoly (2011), Signatures of the Antarctic ozone hole in Southern Hemisphere surface
744 climate change, *Nature Geosc.*, *4*(11), 741–749.

745 Toggweiler, J., et al. (2009), Shifting westerlies, *Science*, *323*(5920), 1434–1435.

746 Trenberth, K. E., and Coauthors (2007), *Observations: Surface and atmospheric climate*
747 *change*, 235–336 pp., S. Solomon et al., Eds., Cambridge University Press.

748 Vianna, M. L., and V. V. Menezes (2013), Bidecadal sea level modes in the North and
749 South Atlantic Oceans, *Geophys. Res. Lett.*, *40*, 5926–5931.

750 Wainer, I., Gent, P., and Goni, G. (2000), Annual cycle of the Brazil-Malvinas Conflu-
751 ence region in the National Center for Atmospheric Research climate system model, *J.*
752 *Geophys. Res.*, *105*(C11), 26167–26177.

753 Wainer, I., Goes, M., Brady, E., and Murphy, L. (2012), Changes in the intermediate
754 Water Mass Formation Rates in the global ocean for the Last Glacial Maximum, Mid-
755 Holocene and Pre-Industrial Climates, *Paleoceanogr.*, *27*, PA3101.

756 Weaver, A. J., M. Eby, E. C. Wiebe, C. M. Bitz, P. B. Duffy, T. L. Ewen, A. F. Fanning,
757 M. M. Holland, A. MacFadyen, H. D. Matthews, et al. (2001), The UVic Earth system
758 climate model: Model description, climatology, and applications to past, present and
759 future climates, *Atmos.-Oc.*, *39*(4), 361–428.

760 You, Y. (2002), Quantitative estimate of Antarctic Intermediate Water contributions from
761 the Drake Passage and the southwest Indian Ocean to the South Atlantic, *J. Geophys.*
762 *Res.*, *107*, 3031.

Table 1. Summary of the climate model experiments.

Experiment	Wind Forcing	CO_2 Forcing
CONTROL	NCEP climatology	1800 level
SAM	NCEP clim plus SAM	1800 level
SAM + NAO	NCEP clim plus SAM plus NAO	1800 level
SAM + NAO + CO_2	NCEP clim plus SAM plus NAO	Transient to 384 ppmV in 2009

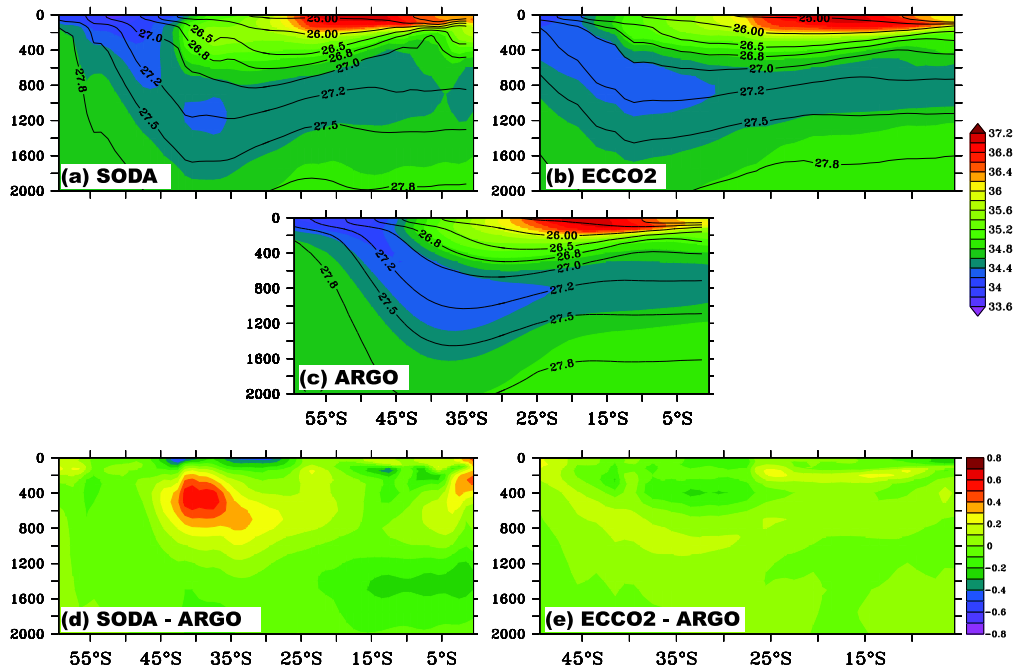


Figure 1. Meridional section of the climatological average (after 2004) of salinity at 25°W in the South Atlantic. Depth is in meters. Relevant potential density surfaces (σ_θ in Kg/m^3) are overlaid. Panel a) is for SODA, b) for ECCO2, c) for Argo climatology [Roemmich and Gilson, 2009], d) SODA - Argo and e) ECCO2 - Argo.

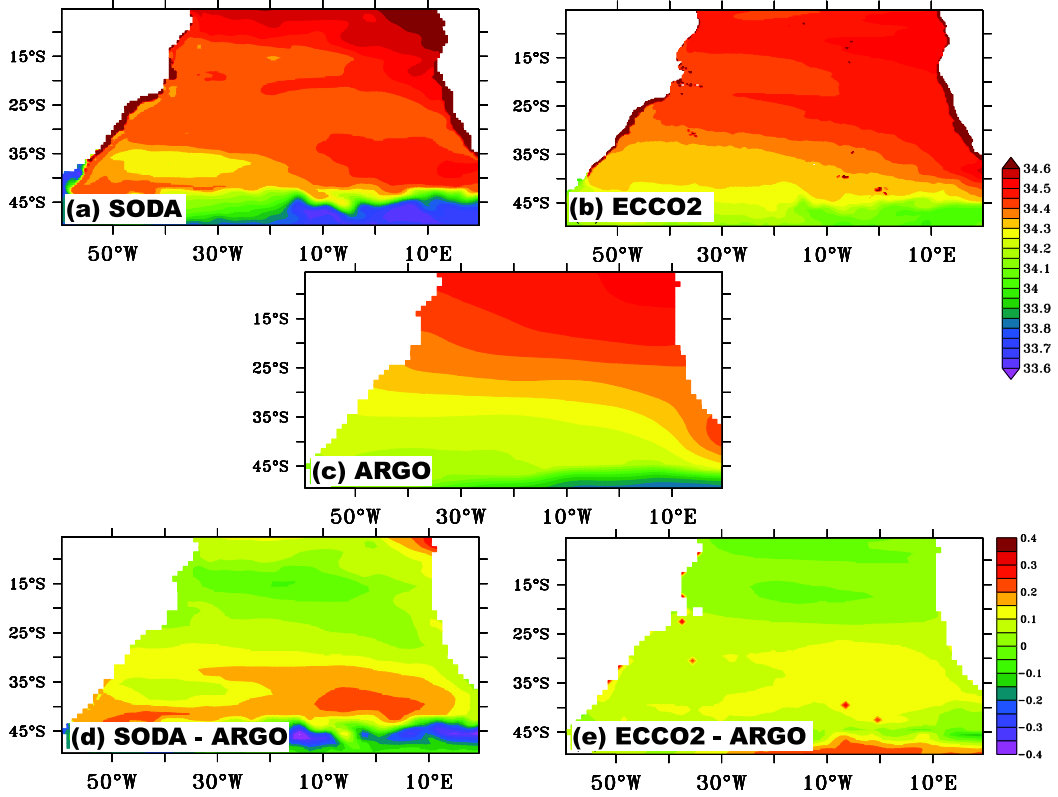


Figure 2. Maps of the climatological average (after 2004) of the salinity minimum surface in the South Atlantic. Panel a) is for SODA, b) for ECCO2, c) for Argo climatology [Roemmich and Gilson, 2009], d) SODA - Argo and e) ECCO2 - Argo.

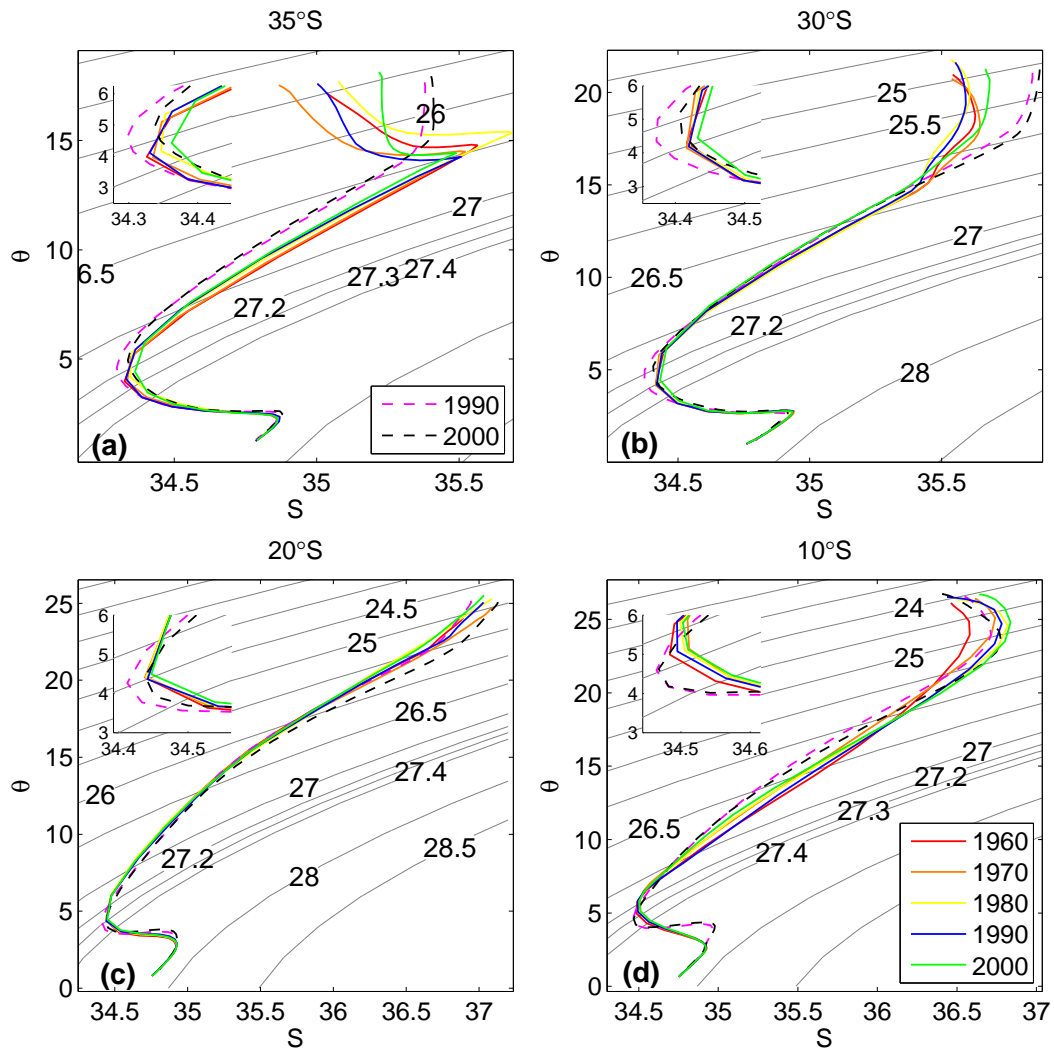


Figure 3. Θ/S diagram for the South Atlantic Ocean at 25°W for a) 35°S , b) 30°S , c) 20°S and d) 10°S . Solid colored lines represent SODA's decadal averages for the 1960s (red), 1970s (orange), 1980s (yellow), 1990s (green) and 2000s (blue). Dashed colored lines represent ECCO2's decadal averages for 1990s (magenta) and 2000s (black).

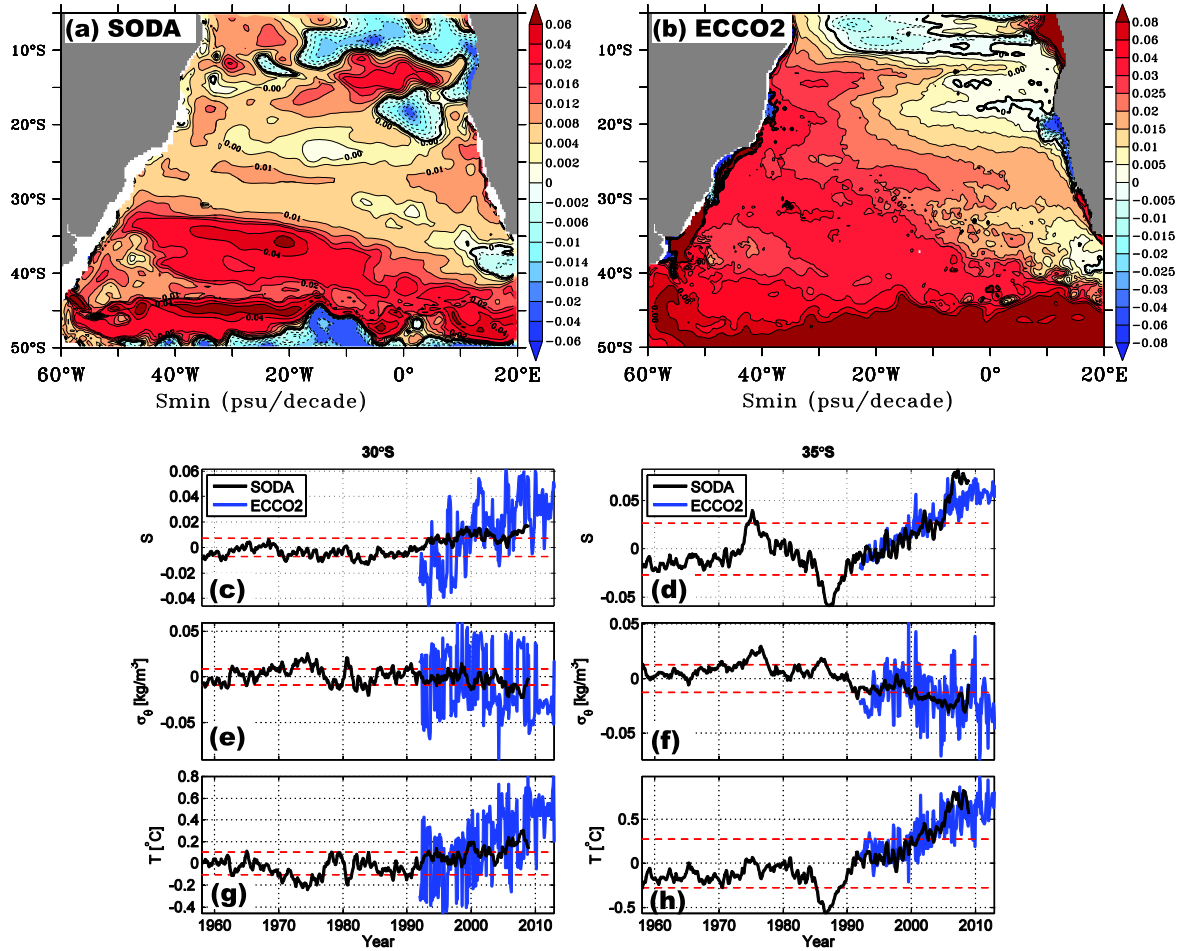


Figure 4. Salinity minimum trend between 1990's and 2000's (psu/decade) for (a) SODA and (b) ECCO2. Panels (c-h) are the time series of the salinity (c, d), sigma density (e,f), and temperature (g,h) anomalies with respect to SODA's 1960-2008 period at the location of the salinity minimum. Timeseries on the left column are for 25°W/30°S and on the right column for 25°W/35°S. Black timeseries is for SODA and blue is for ECCO2. The red dashed lines represent SODA's the three standard deviation levels relative to each parameter.

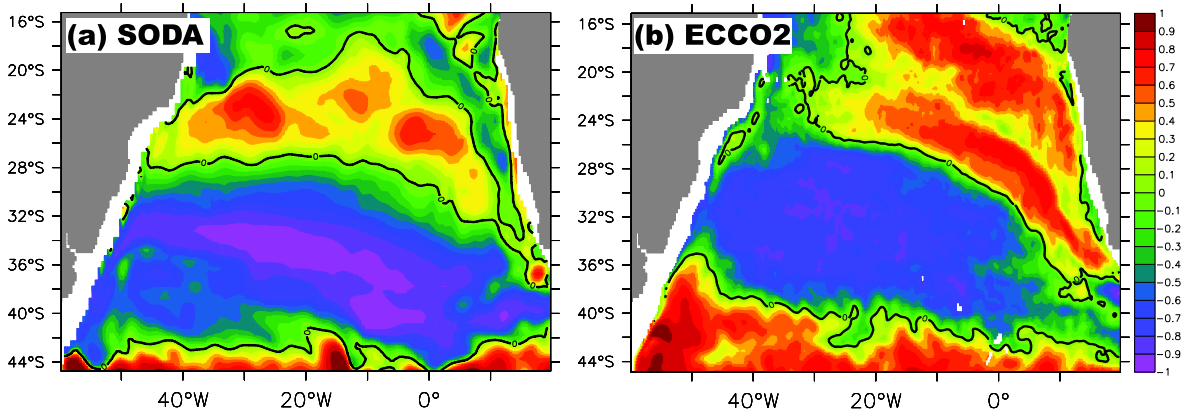


Figure 5. Correlation between the components of the sigma density, i.e., thermopycnal and halopycnal components, at approximately 1100 m depth for (a) SODA and (b) ECCO2. The components of sigma are calculated by keeping the other component as the climatological value.

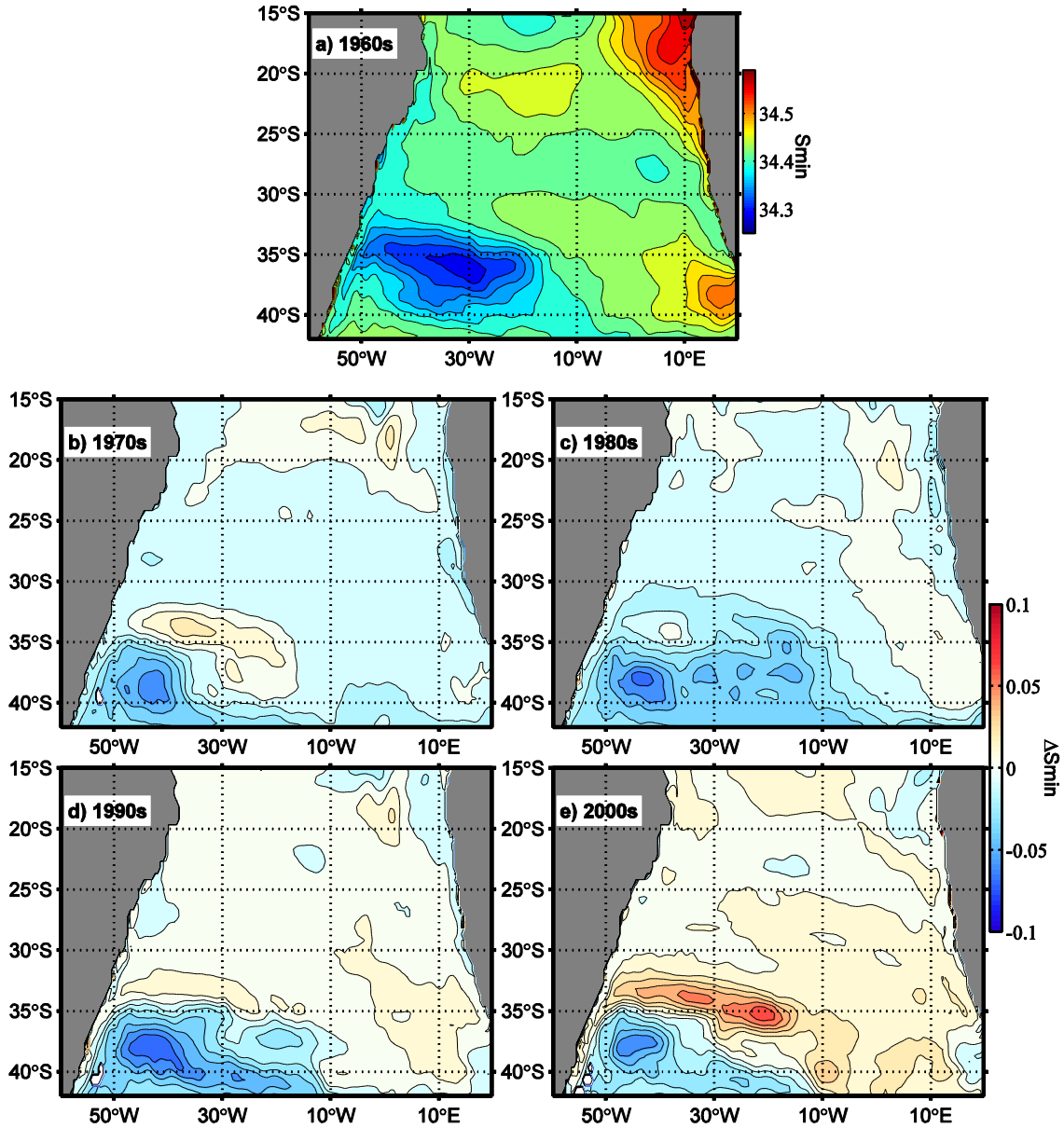


Figure 6. Salinity minimum within the layer defined by the $\gamma_n = 27.1$ and $\gamma_n = 27.6$ neutral surfaces for a) 1960s, and anomalies relative to 1960s for b) 1970s, c) 1980s, d) 1990s and e) 2000s.

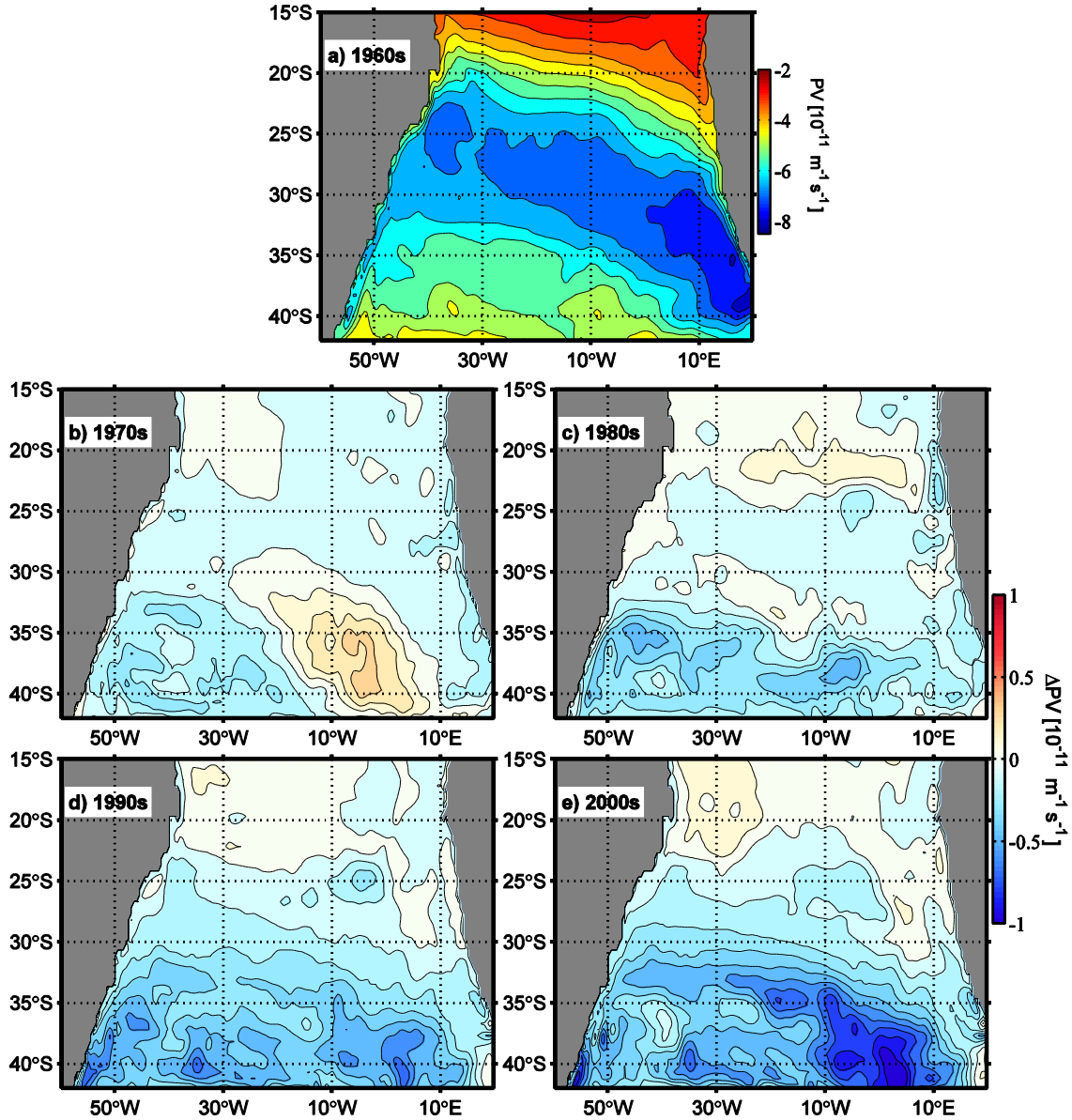


Figure 7. Ertel's potential vorticity calculated within the layer defined by the $\gamma = 27.1$ and $\gamma = 27.6$ neutral surfaces for a) 1960s, and anomalies relative to 1960s for b) 1970s, c) 1980s, d) 1990s and e) 2000s.

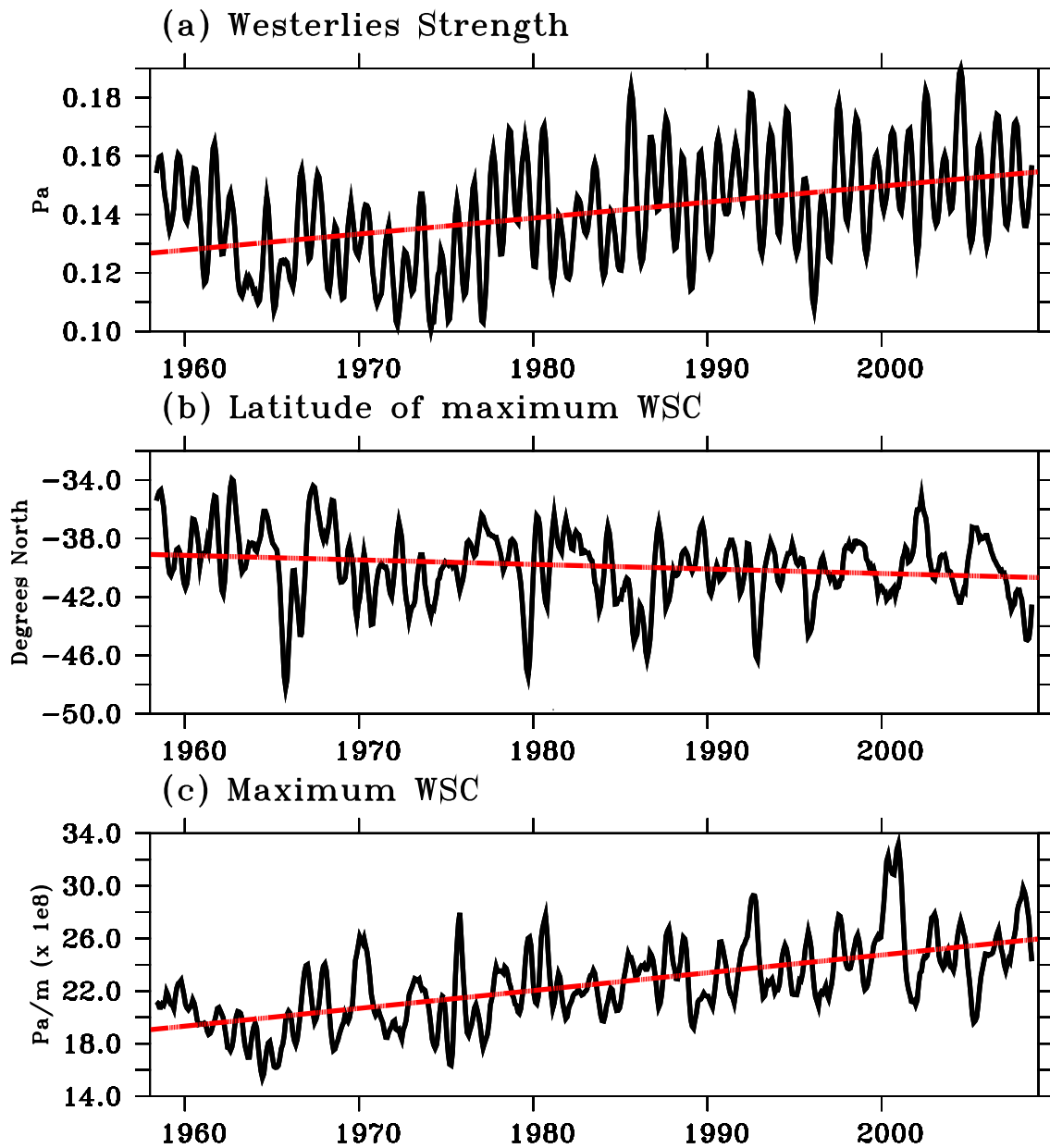


Figure 8. SODA wind stress indices for the eastern South Atlantic ($0\text{--}20^\circ\text{E}$) of (a) westerlies strength (Pascal), (b) latitude of the maximum zonal average wind stress curl (degrees north), and (c) maximum zonal average wind stress curl ($\text{Pascal}/\text{meter} \times 1e^{-8}$). Linear regressions are overlaid in red.

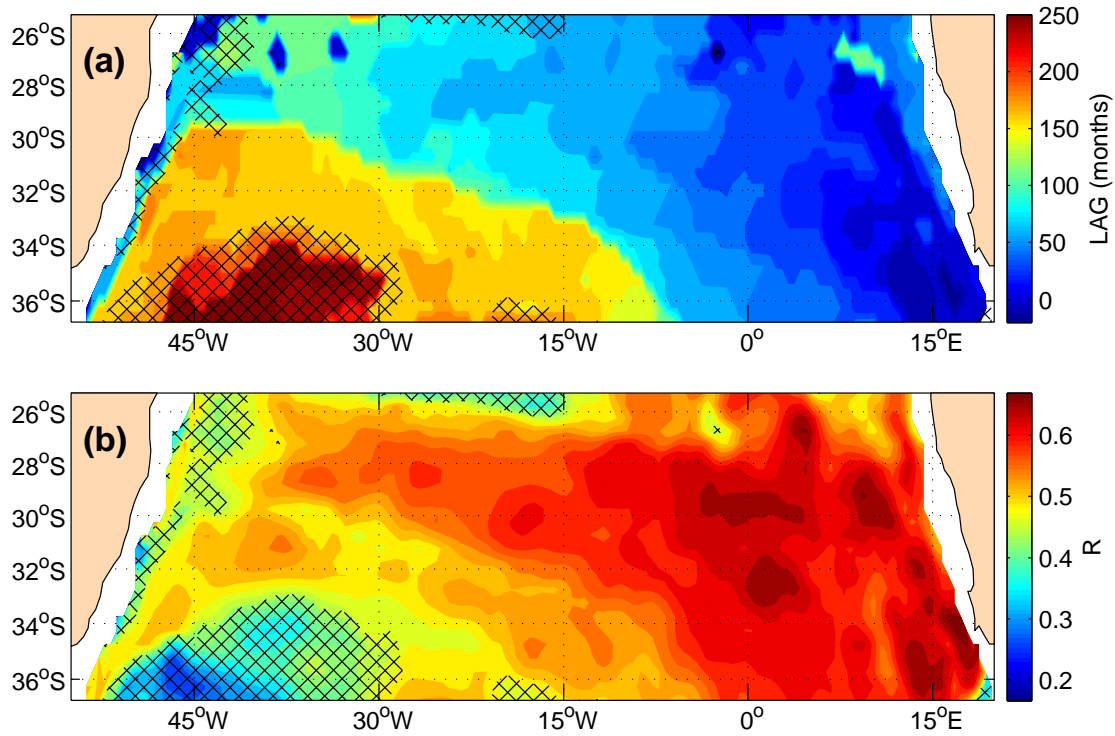


Figure 9. Maximum lagged correlation between the salinity at $\sigma_\theta = 27.2$ and a westerly wind strength index in the southeastern Atlantic, defined by the τ_x averaged between 35°S–65°S/0°E–20°E. (a) is the lag of the maximum correlation (months) and (b) is the maximum correlation. The crossed areas are where correlation values of the pre-whitened timeseries are not statistically significant.

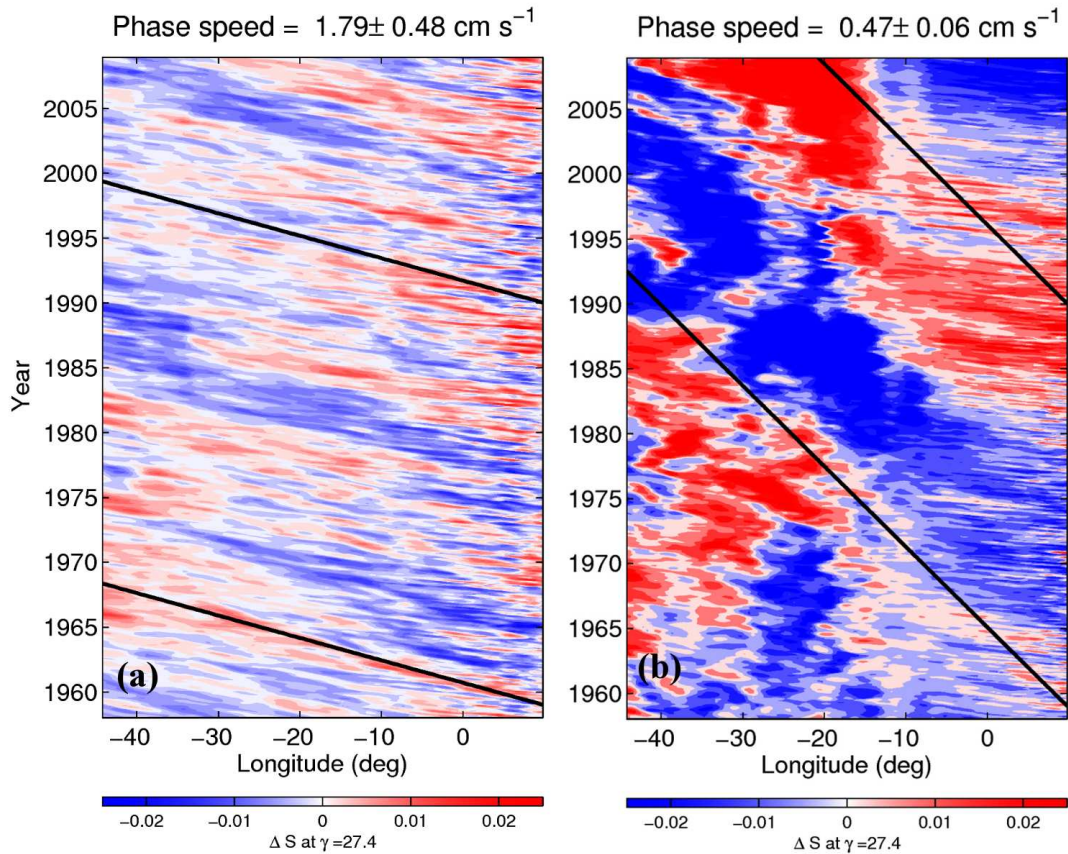


Figure 10. Time x Longitude diagram for the salinity anomalies projected onto the neutral density surface $\gamma_n = 27.4$, that defines the region of minimum salinity in the subtropical Atlantic at (a,c) 30°S and (b,d) 35°S . Panels (a,b) are for SODA and (c,d) are for ECCO2. Following *Barron et al.* [2009], the zonal average of the salinity anomalies is subtracted from the diagrams to highlight the propagating features. The phase speed calculated from the method of *Barron et al.* [2009] is shown on the top of each panel and its displacement is shown as a black line overlaid on the contours.

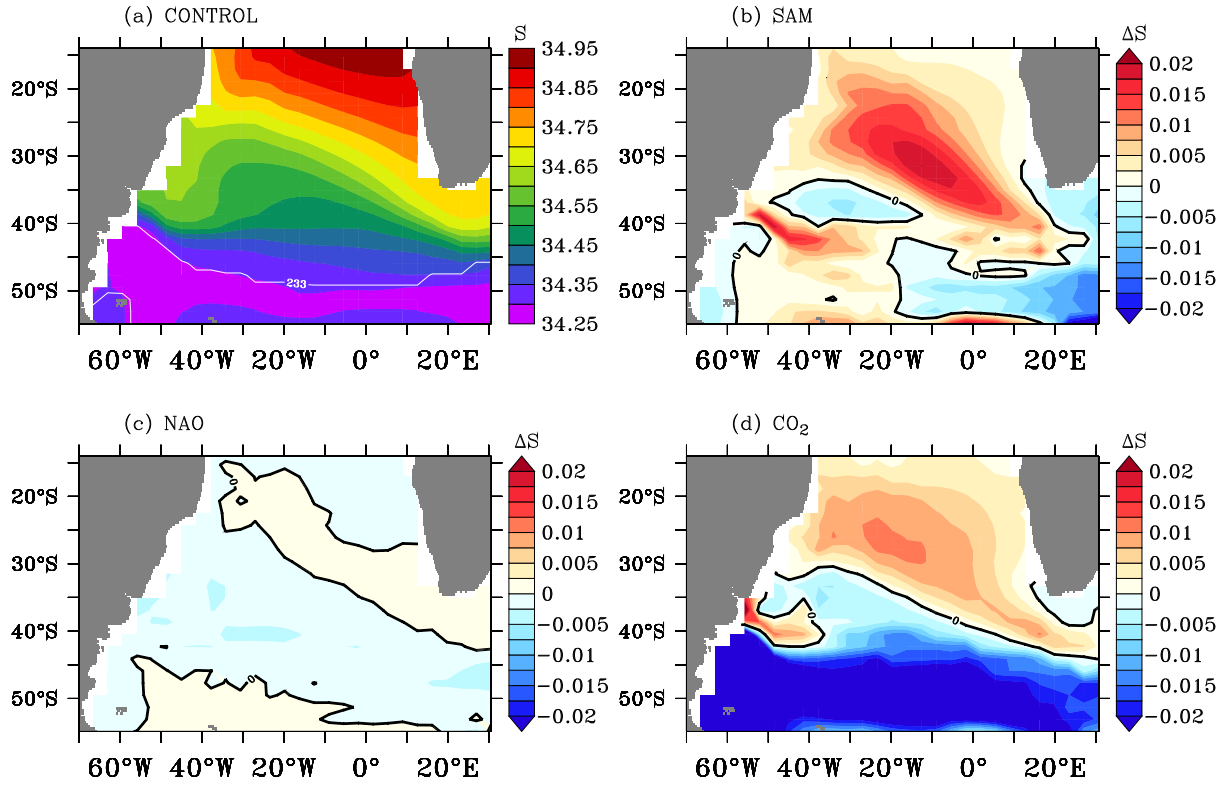


Figure 11. (a) South Atlantic salinity minimum in the Uvic CONTROL experiment averaged between 2000–2009. (b–d) Average (2000-2009) salinity minimum differences among the experiments, in which each panel shows how adding one forcing changes the salinity in comparison to the experiment without that forcing, for (b) SAM, (c) NAO, and (d) CO₂.

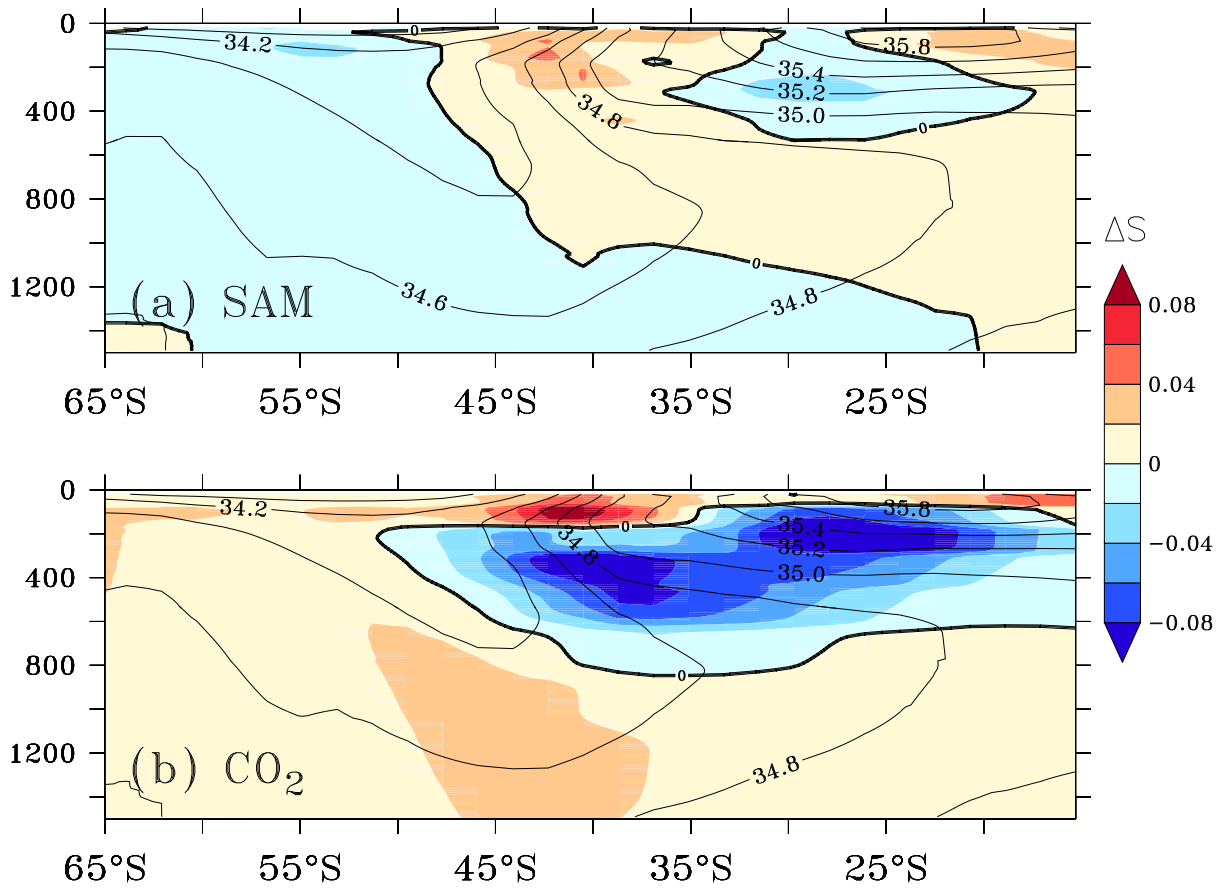


Figure 12. Meridional sections of salinity anomalies (psu) in the Atlantic Ocean for the period 2000 to 2009 for the UVic experiments forced by (a) SAM and (b) CO₂. Overlaid black contours are the sigma-averaged salinity in the section. The salinity anomalies are differences along isopycnals that have been remapped to depth levels.

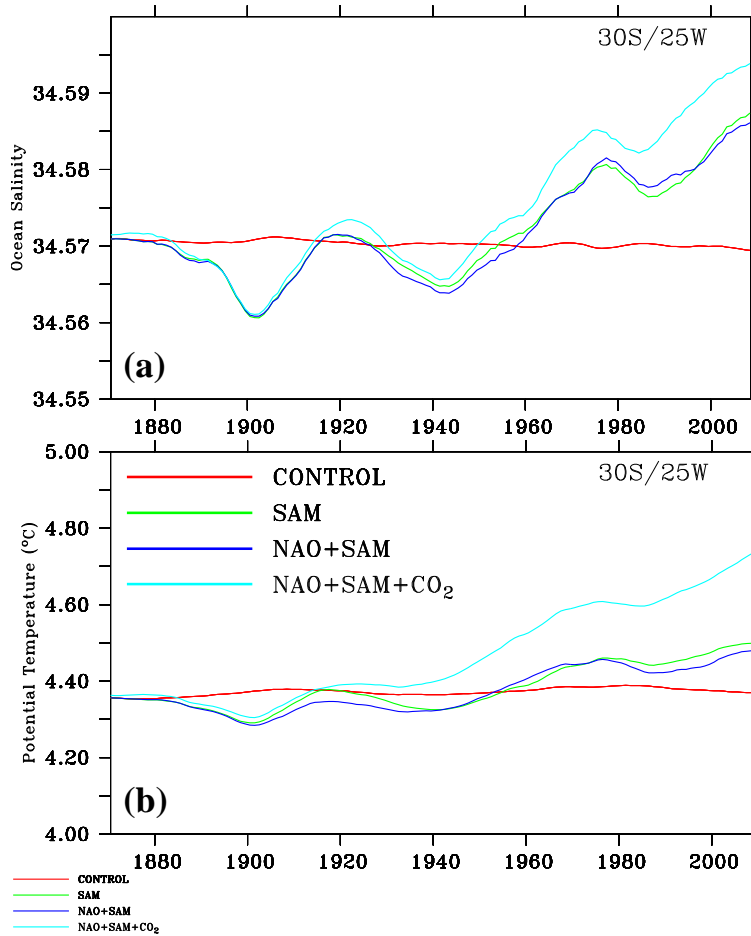


Figure 13. Time series of (a) salinity and (b) potential temperature **at the salinity minimum depth at 30°S/25°W from the UVIC model experiments.** The colored lines are for the CONTROL (red), SAM only (green), SAM plus NAO (dark blue), and NAO plus SAM plus CO₂ (cyan) experiments.

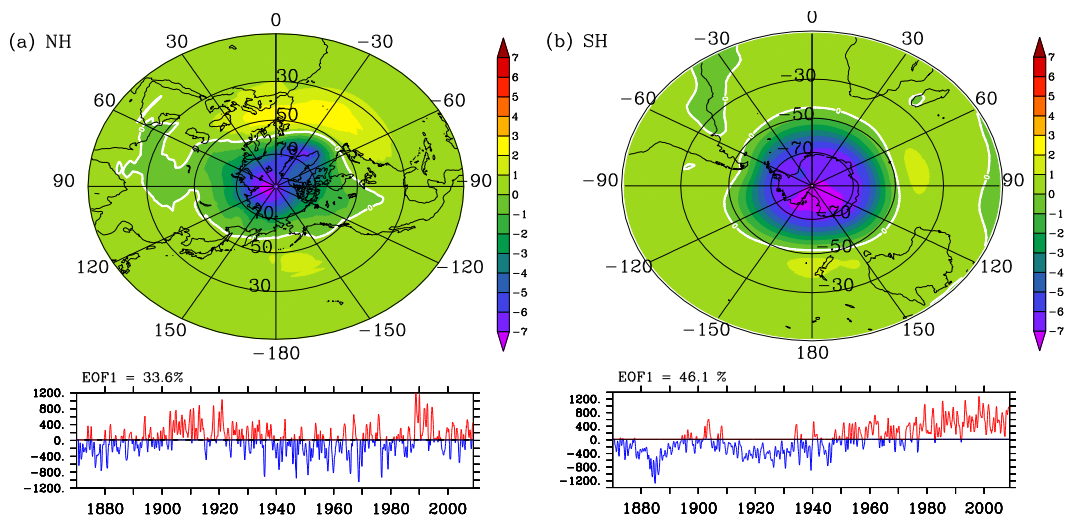


Figure 14. First EOF of the hemispheric sea level pressure used to force the atmospheric model in UVic for the (a) Northern Hemisphere and (b) Southern Hemisphere.